Doctoral Dissertations and Master's Theses

Spring 4-2017

A Feasibility Study for Using the ERAU Échelle Spectrograph to Improve Orbital Parameters of Spectroscopic Binary Systems

Stanimir Letchev
Embry-Riddle Aeronautical University

Follow this and additional works at: https://commons.erau.edu/edt

Part of the Engineering Physics Commons, and the Stars, Interstellar Medium and the Galaxy Commons

A FEASIBILITY STUDY FOR USING THE ERAU ÉCHELLE SPECTROGRAPH TO IMPROVE ORBITAL PARAMETERS OF SPECTROSCOPIC BINARY SYSTEMS

BY

STANIMIR LETCHEV

A Thesis

Submitted to the Department of Physical Sciences

and the Committee on Graduate Studies

In partial fulfillment of the requirements

for the degree of

Master in Science in Engineering Physics

04/2017

Embry-Riddle Aeronautical University

Daytona Beach, Florida

A FEASIBILITY STUDY FOR USING THE ERAU ÉCHELLE SPECTROGRAPH TO IMPROVE ORBITAL PARAMETERS OF SPECTROSCOPIC BINARY SYSTEMS

by

Stanimir Letchev

This thesis was prepared under the direction of the candidate's Thesis Committee Chair, Dr. Jason Aufdenberg, Associate Professor, Daytona Beach Campus, and Thesis Committee Members Dr. Edwin Mierkiewicz, Assistant Professor, Daytona Beach Campus, and Dr. Anthony Reynolds, Associate Professor, Daytona Beach Campus, and has been approved by the Thesis Committee. It was submitted to the Department of Physical Sciences in partial fulfillment of the requirements of the degree of Master of Science in Engineering Physics
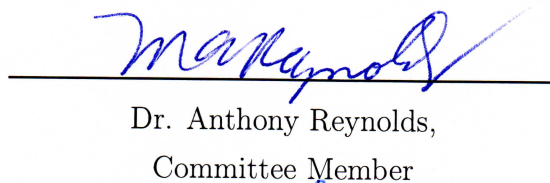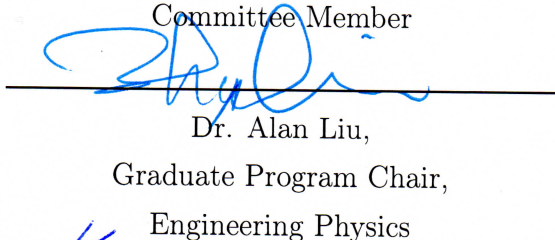
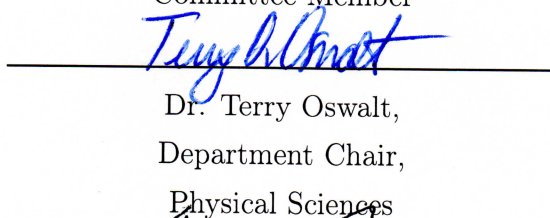THESIS COMMITTEE:
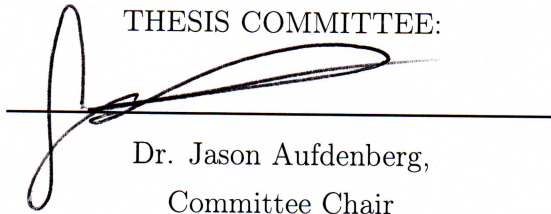
Dr. Jason Aufdenberg,
Committee Chair

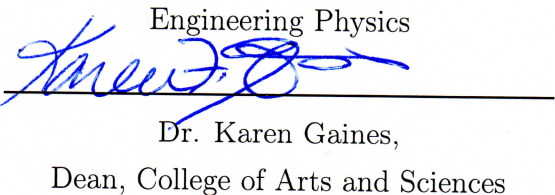Dr. Edwin Mierkiewicz,
Committee Member
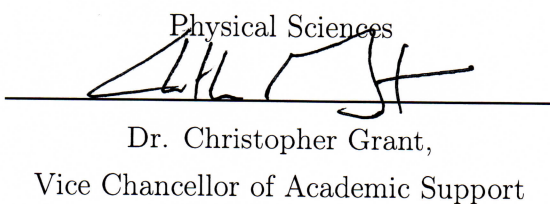
Dr. Anthony Reynolds,
Committee Member

Dr. Alan Liu,
Graduate Program Chair,
Engineering Physics

Dr. Terry Oswalt,
Department Chair,
Physical Sciences

Dr. Karen Gaines,
Dean, College of Arts and Sciences

Dr. Christopher Grant,
Vice Chancellor of Academic Support

iii

Abstract

Binary stars are critical for establishing knowledge of stellar masses and refining the mass-luminosity relationship when used in conjunction with precise parallax measurements. However, many spectroscopic binaries have poorly defined orbital parameters as they have not been revisited with newer CCD technology since their first observations on photographic plates. This thesis examines the feasibility of using the high-resolution échelle spectrograph at Embry-Riddle Aeronautical University (ERAU) to obtain radial velocities of spectroscopic binary stars, and establishes a software pipeline to obtain their orbital parameters. This was done by looking at the double-lined binaries HD 205539 and ι Pegasi, as well as the single-lined binary ζ Andromedae. Twenty-five nights of data were taken from October 18th, 2016 to December 18th, 2016. These data were cross correlated against the radial velocity standards ι Piscium and α Cassiopeiae. A two-dimensional cross-correlation algorithm created by Zucker and Mazeh [1994] was translated into MATLAB and was used to calculate the radial velocities for the double-lined systems, and a MATLAB cross-correlation algorithm was implemented to do the same for the single-lined system. Orbital parameters were found using the Spectroscopic Binary Solver from Johnson [2004] that match previously determined parameters, derived from independent data, to within two standard deviations. It can be concluded that the spectrograph and data analysis pipeline has sufficient accuracy and precision to be used for further studies into spectroscopic binary systems.

Acknowledgments

Thank you to Drs. Aufdenberg, Mierkiewicz, and Reynolds for their immense help in revising this thesis. A thank you as well to Dr. Davenport for his IDL implementation of the TODCOR algorithm, Delwin Owen Johnson for his work on the SBS software, and Mr. Damon Burke, Observatory Engineer, for keeping the telescope systems in good working order during the observing runs.

Contents

List of Tables

List of Figures

Chapter 1

INTRODUCTION

Binary star systems are among the most important objects studied observationally (Batten [1973]). This is because they provide important information about stellar masses that cannot be obtained as easily from other methods such as the less-constrained mass-luminosity relation, and precise stellar parallaxes are the exception, not the norm, at least until the Gaia survey is complete. Stellar mass is a very important parameter that allows us to understand the evolutionary track and age of a star.

In order to determine the constraints on mass given by a stellar orbit, the orbital parameters must be determined. These parameters, combined with orbital equations and Kepler's third law, can then be used to calculate stellar masses. However, the confidence level of the masses found is then directly linked to the confidence level of the orbital parameters. Therefore, we strive for the highest accuracy and precision possible for these parameters.

While some binary star systems can be resolved visually through astrometry, many more binary systems are simply too distant or too close together to be visually resolved. For some of these systems, their orientation allows the stars to eclipse each other, letting us measure the brightness dips and determine inclinations. However, this is rare, so we turn to different methods in order to detect these systems and determine their orbital parameters.

Spectroscopy is a useful method for measuring the radial velocity shift that is

caused by the motion of each star about the system's center of mass. Instead of being constrained by angular resolvability or inclination, we are limited by the magnitude of the Doppler shift in the spectral lines of the star(s) and the brightness of the system due to the dispersion of light in the spectrograph.

There are two types of spectroscopic binary star. A double-lined system has both stars' spectra clearly visible in a spectroscopic measurement. This allows for the separate measurement of the Doppler shifts of each star, giving two radial velocity measurements. This type of system, depending on the relative brightness of the spectra, also allows for the spectral classification of both stars. A single-lined system, however, has only one spectrum visible. The secondary star's spectrum is too faint compared to the primary's. For this type of system, only one radial velocity measurement can be made, and only one stellar spectrum can be identified.

Over 3500 stars have been cataloged as spectroscopic binaries, and many studies have been done to determine these stars' orbital parameters since the advent of spectroscopy using photographic plates at the end of the 19th century (Pourbaix et al. [2009]). However, modern advances in spectrographs with higher resolution and increased sensitivity of CCD technology have allowed us to make increasingly improved measurements of these orbits (Gray [1992]).

The 9th Catalogue of Spectroscopic Binary Orbits compiled by Pourbaix et al. [2009] contains a comprehensive list of known spectroscopic binaries including their orbital parameters and archival radial velocity data from the original sources. The compilers of this catalog also assign a grade to each entry, reflecting the quality of the data and certainty of the orbital parameters, 5 being the best and 0 the worst (Pourbaix et al. [2009]).

The observations collected for this thesis were used to establish a software pipeline to determine binary stars' orbital parameters using spectrographic data. These observations were obtained using a fiber-fed échelle spectrograph attached to a 1-meter telescope at Embry-Riddle Aeronautical University. This is the first of a series of observations using this technique, and will serve as a proof-of-concept.

The primary stars for this study were HD 205539, iota Pegasi (ι Peg), and zeta Andromedae (ζ And). The latter two stars were chosen because they were grade 5

standards, meaning their orbital parameters were determined to a high degree of certainty. This allowed for the testing of the various techniques employed in the analysis. ι Peg was chosen due to its similarity in spectral type to HD 205539, and ζ And was chosen for its simplicity, due to its plentiful spectral lines as a K-type star and its single-lined nature. HD 205539, or HR 8257, was originally chosen as the primary target of the study, as its reference in the SB9 catalog only cited an original study done by Harper [1925], suggesting that the orbital parameters could be significantly improved. Several other factors made it an appealing target for observation. Its 6th magnitude brightness ensured a reasonable signal from the star, and its cooler F spectral type allowed for more spectral lines to be identified than the many A-type stars with grade 3 or lower orbital determinations. Unfortunately, it was discovered that a comprehensive study of the star was published in 2009 by Fekel et al. [2009]. This effectively turned HD 205539 into another grade 5 standard that could be analyzed.

In the remainder of this thesis, the instrumentation used to obtain the spectrographic data will be discussed, the observing strategy will be outlined, the data reduction and analysis will be detailed, followed by a discussion of the results and conclusion.

Chapter 2

INSTRUMENTATION

2.1 Échelle Spectrograph on the 1-Meter Telescope

2.1.1 Spectrograph Mechanics and Installation

The 1-meter telescope at Embry-Riddle Aeronautical University's College of Arts and Sciences building on the Daytona Beach campus was used for all observations taken in this analysis. The telescope was useful due to a large amount of available observing time, allowing for higher cadence observations. The fiber optics and spectrograph were installed in December of 2015.

The eShel Spectrograph used in this thesis was manufactured by Shelyak Instruments. As an échelle-type spectrograph, it uses two different dispersion mechanisms; an initial grating, and a prism to separate the spectral orders. These can clearly be seen in Figure 2.1. It has a documented resolution of $R \gtrsim 10000$, which results in a radial velocity precision of approximately 25 km/s at Hα (6563Å). Additional reduction techniques are required to analyze lower-amplitude velocity shifts, which are detailed further in Subsection 2.1.3 and Chapter 4.

The advantage of this spectrograph is that it is fed by an optical fiber instead of being attached directly to the telescope. This reduces stress and vibrations that would affect the spectrograph's calibration and stability. The spectrograph itself is located in a cabinet in the College of Arts and Sciences fifth floor, underneath

the telescope itself. The cabinet contains a fan that keeps its temperature constant within 1°F throughout all of the observations taken, further reducing variations in measurements.

The spectrograph is wavelength calibrated with a Thorium-Argon (Th-Ar) hollow-cathode lamp. Tungsten and LED lamps are also in the calibration unit, shown in Figure 2.2, and are used for providing a flat-field for the Shelyak AudeLA data collection and reduction software to normalize the sensitivity variation across each order (Cochard and Thizy [2011]). In order to ensure that the calibration lamps and starlight follow the same optical path, the light from the lamps is directed through a 200 micron optical fiber to the fiber injection and guider unit (FIGU), which has an internal mirror that can be flipped into or out of place to shine either starlight or a calibration light into the 50 micron optical fiber the carries light to the spectrograph.

2.1.2 CCD Cameras

All of the spectrograph's images were taken using an SBIG STT-1603 CCD camera. The SBIG CCD was attached to the top of the spectrograph and controlled by the AudeLA software. During all observations, the CCD was first cooled to -35°C to reduce dark current.

In addition, a CCD guide camera, an Atik Titan, with a plate scale of 0.127 arcseconds/pixel providing a 1.4 by 1.0 arcminute field of view around the fiber, was mounted to the side of the FIGU (labeled 3 in Fig. 2.2) This camera was used to look at the mirror inside the FIGU so that a star could be correctly positioned on the optical fiber leading to the spectrograph. Using the Maxim DL software in conjunction with this camera allowed for both obtaining continuous images of the internal mirror and for tracking the star itself.

2.1.3 Spectrograph Calibration

Looking for the small shifts in spectral lines caused by binary stars and exoplanets requires careful wavelength calibration of the spectrograph in order to achieve accurate and precise radial velocities. Several techniques were employed to achieve sub-pixel
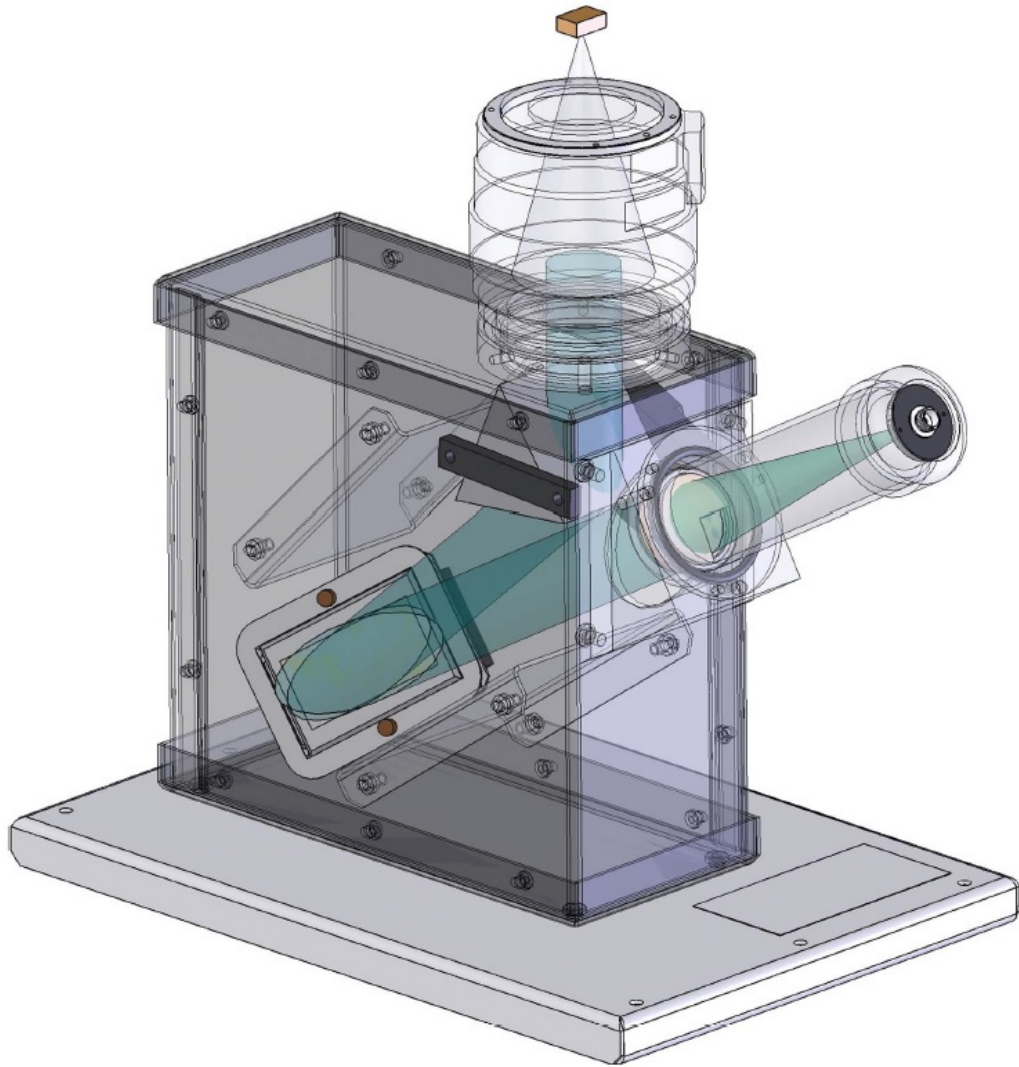
Figure 2.1: The light path inside the eShel spectrograph (Eversberg [2016]).

Figure 2.2: The eShel Spectrograph's main parts. Clockwise from top: telescope mount, spectrograph, FIGU. The fiber labeled 4 leads to the calibration unit. The fiber labeled 2 leads to the spectrograph (Cochard and Thizy [2011]).
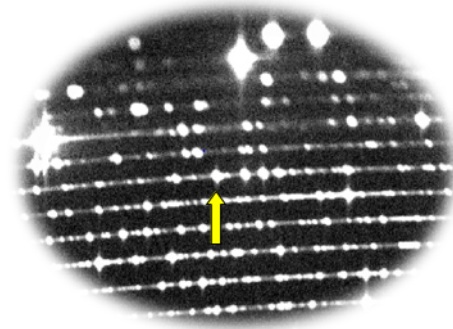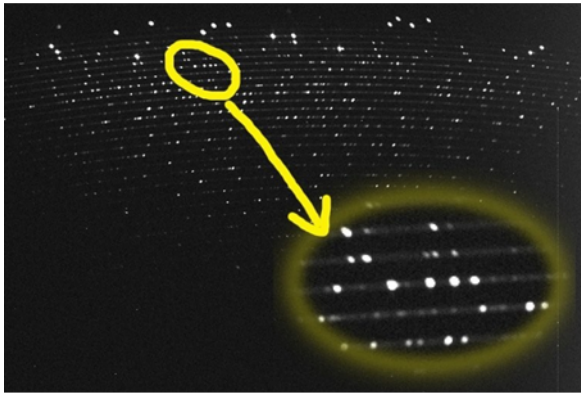
Figure 2.3: The Th-Ar Pattern required for the AudeLA calibration (Cochard and Thizy [2011]).

resolution. Having a very well-calibrated spectrum allows us to determine the shifts in the spectrum more accurately. In addition, cross-correlating the spectra with known velocity standards allows us to detect the shifts beyond the resolving power of the spectrograph by using a statistical analysis: looking at all of the absorption lines as opposed to only one line. Using an average of the shifts of all the spectral lines in 17 orders of the echelle spectrum gives higher precision than one line alone.

Wavelength calibration is done automatically through the pre-packaged AudeLA software. This requires several input parameters, however. The first step in the wavelength calibration is to take a test image of the Th-Ar spectrum and look for the easily-recognizable set of lines shown in Fig. 2.3. The x and y coordinates of the leftmost emission line are input into the software's Instrument Setup, shown in Fig. 2.4.

These coordinates are only part of the parameters the AudeLA software requires to perform a thorough wavelength calibration. It also requires information about the spectrograph setup. There are several angles that must be known, as shown in Figure 2.6. These numbers allow the AudeLA software to predict where the Th-Ar emission lines will appear on the image so that it can locate and identify them. However, the software defines these angles differently from the standards in échelle spectroscopy. While α is consistent, the software angle β is analogous to θ in Figure 2.6. This angle
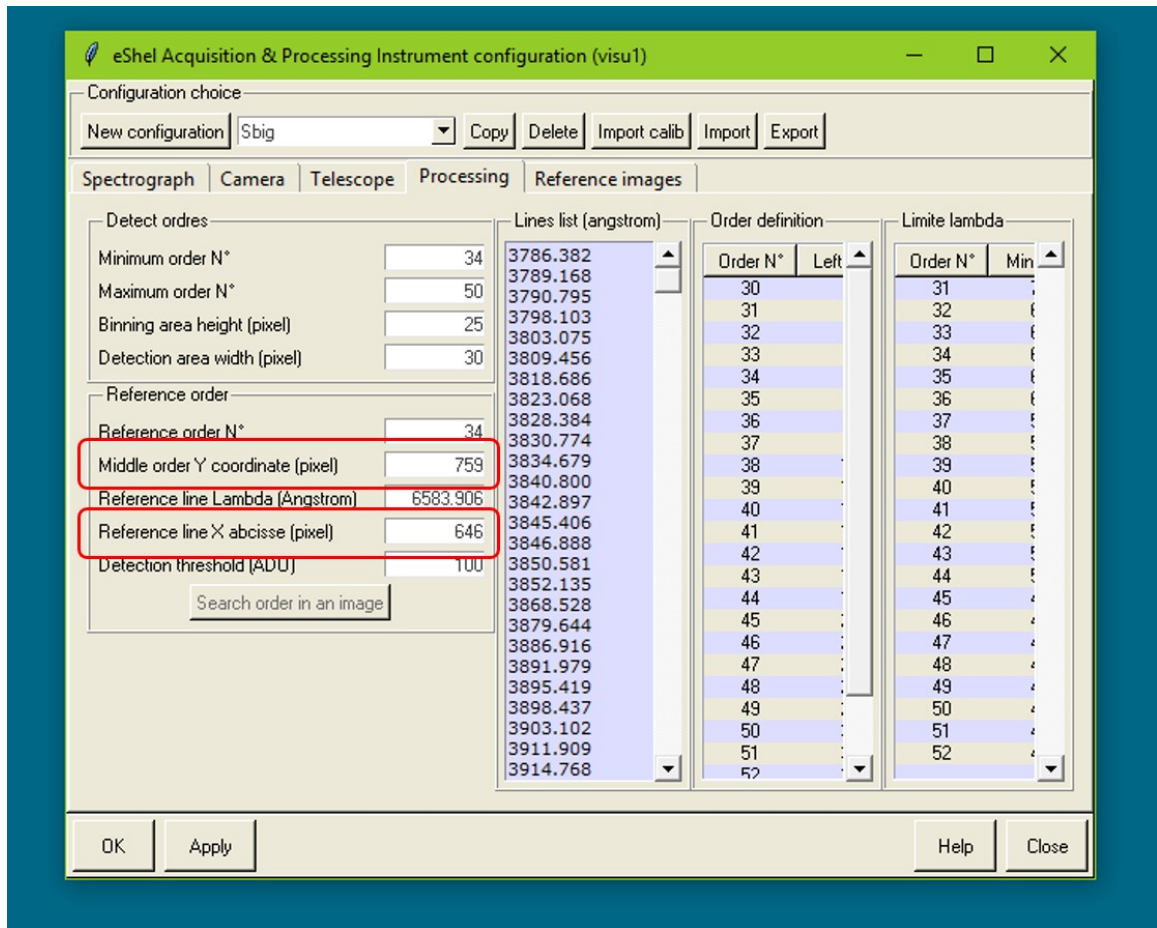
Figure 2.4: The location of the reference line input in the AudeLA software(Cochard and Thizy [2011]).
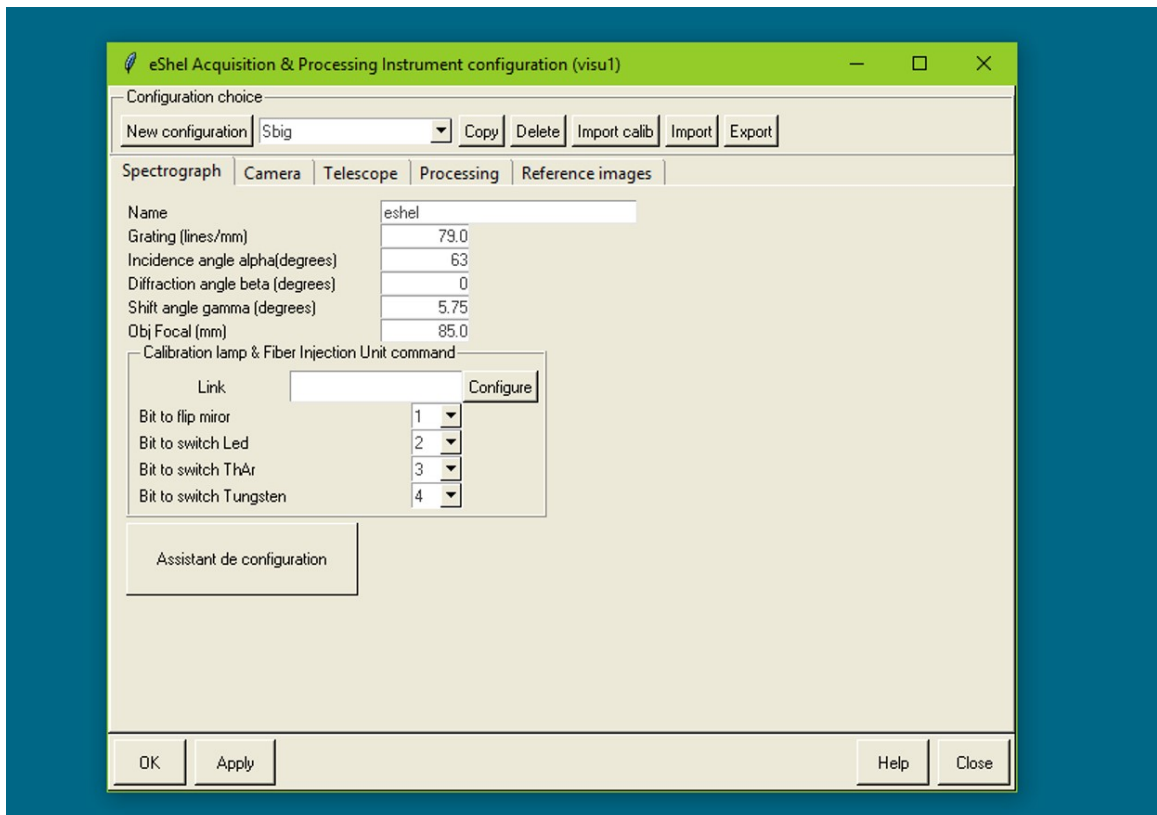
Figure 2.5: The location of the spectrogrpah angle input in the AudeLA software.
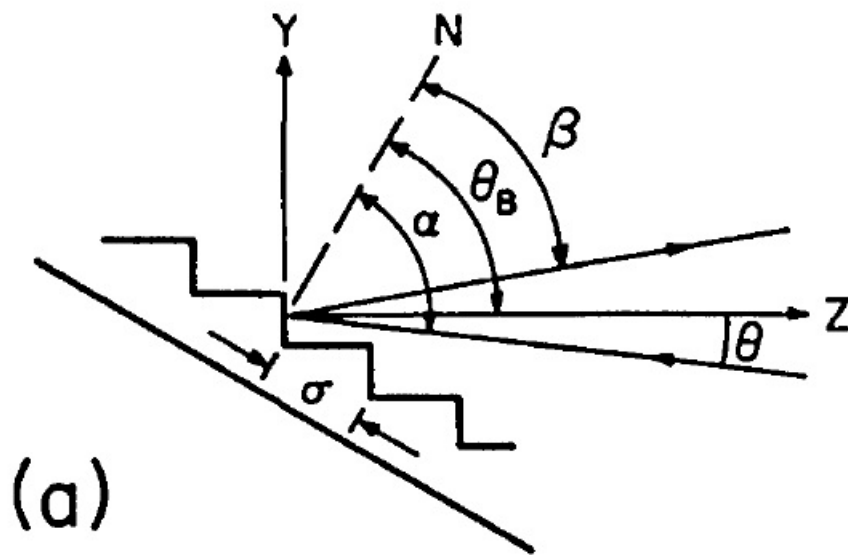
Figure 2.6: A diagram showing the angles used as spectrograph parameters (Schroeder and Hilliard [1980]).
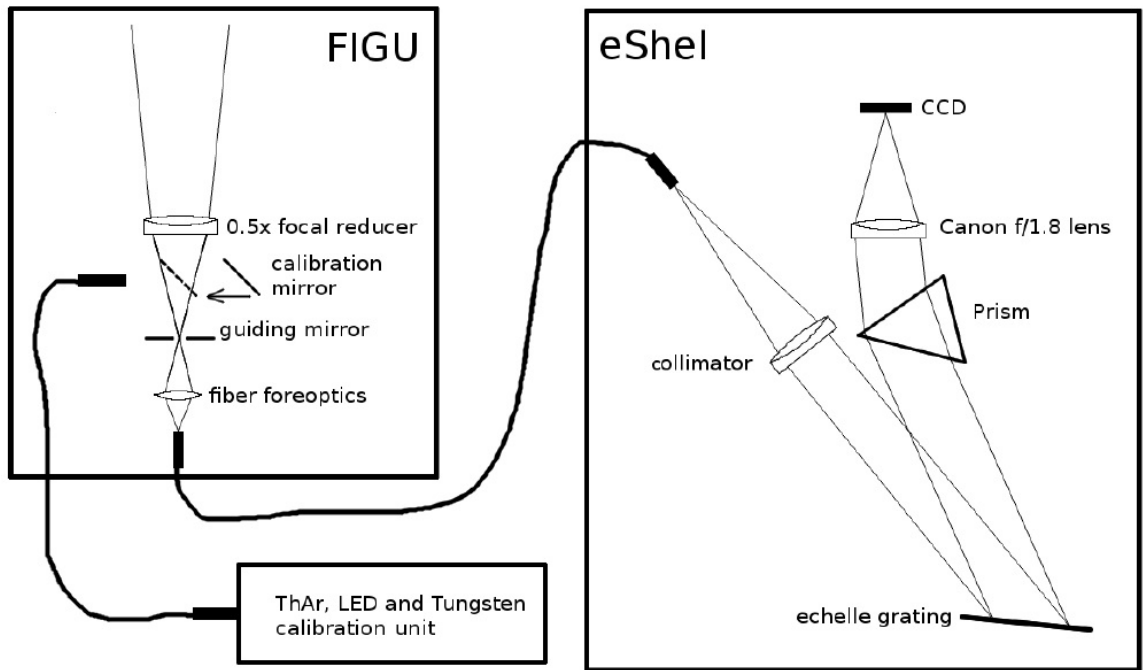
Figure 2.7: The light path of the eShel from a top-down perspective (Pribulla et al. [2015]).

Table 2.1: The AudeLA calibration output, showing the RMS of each order, its central wavelength, the rms-cal values, resolution (calculated by the width of each emission line), and the number of lines the software locates in the order. The central wavelength of each order is $\lambda_c = 2\frac{\sigma}{m} \sin\alpha \cos\gamma$ where m is the order number and σ is the échelle groove spacing, 79 grooves mm^{-1}.

ORDER	RMS	CENTRAL (Å)	RMS-CAL	RESOLUTION	NB LINE
34	0.018	6606.44	0.0105	11115.7	13
35	0.0163	6417.684	0.0152	12043.9	15
36	0.0147	6239.415	0.0083	12689.4	15
37	0.0132	6070.782	0.0102	12525	14
38	0.0136	5911.025	0.0223	12283.1	16
39	0.0141	5759.46	0.0158	12794.7	18
40	0.0142	5615.474	0.0079	12757.2	11
41	0.0151	5478.511	0.0181	12344	18
42	0.0156	5348.07	0.0474	11420.5	17
43	0.0152	5223.696	0.0122	12256.2	16
44	0.0147	5104.976	0.0252	12073.6	14
45	0.0139	4991.532	0.0177	12307.3	13
46	0.0127	4883.021	0.0305	11972	14
47	0.0117	4779.127	0.0143	12869.1	10
48	0.0113	4679.561	0.0052	12442.4	11
49	0.0126	4584.06	0.0366	12028.5	11
50	0.0181	4492.379	0.007	11433.7	7

is defined to be 0, due to the fact that the eShel is a quasi-Littrow design, described in Schroeder and Hilliard [1980]. In addition, what the AudeLA software refers to as γ is the out-of-plane angle by which the light is shifted after hitting the grating so that it heads toward the prism. This shift is shown in Figure 2.7. The ideal parameters for our setup were $\alpha = 62.7°$ and $\gamma = 5.75°$. These were found by adjusting these parameters until the difference between the calculated and actual lines (given as the rms-cal values) in each order was minimized, as shown in Table 2.1. This occurred when the predicted locations of the Th-Ar emission lines overlapped well with their observed locations, as shown in Figure 2.8.
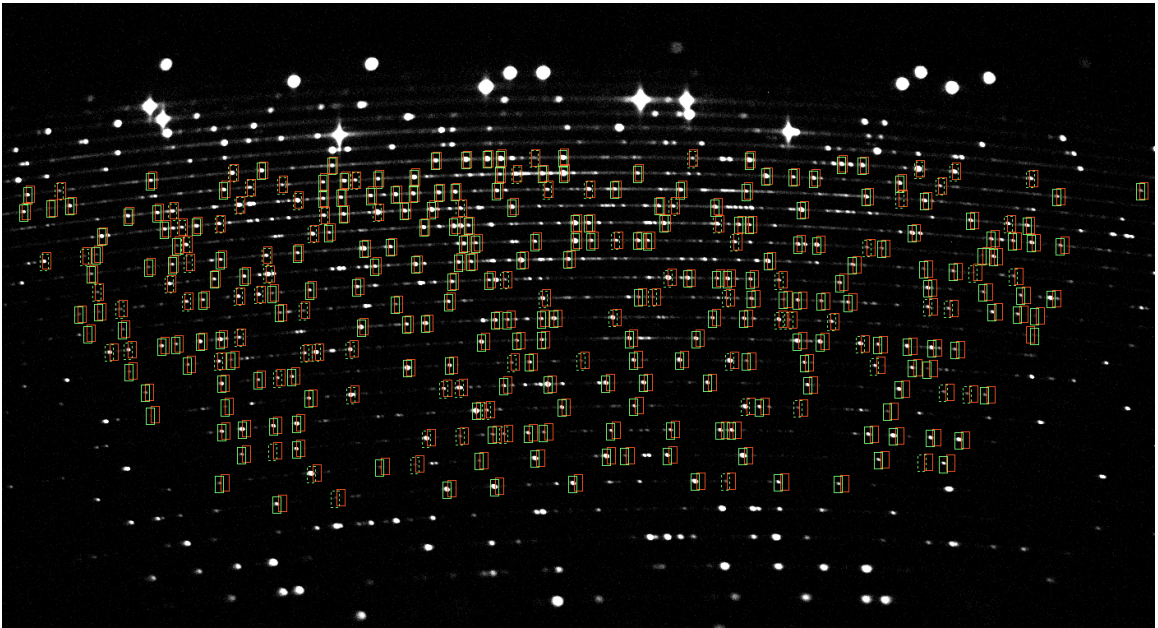
Figure 2.8: The AudeLA Th-Ar calibration output in image form. The red boxes indicate where the AudeLA software calculated the Th-Ar lines should be located, and the green boxes indicating where the lines were found.

Chapter 3

OBSERVATIONS

3.1 Stars Observed

3.1.1 Radial Velocity Standards

In order to set a zero point for the magnitude of the observed Doppler shift, stars that have well-defined and unchanging radial velocities were observed and analyzed. These stars' spectra were used in the cross correlation technique which is described in Chapter 4. They also are used to assess the stability of the spectrograph calibration from night to night. This stability can be seen in Figure 3.1, which shows that the spectra of the radial velocity standards do not shift substantially throughout our observing run. The larger errors for ι Psc may be due to its reduced number of spectral lines compared to α Cas.

Two main radial velocity standards, found using *The Astronomical Almanac* for 2015, were used in this analysis. They are detailed in Table 3.1. They were chosen based on spectral type similarity to the spectroscopic binary stars and for ease of observation due to their brightness and location on the sky. For the K-type ζ And,

Table 3.1: Stellar properties for the radial velocity standard stars observed.

Name	HD No.	α	δ	Epoch	V Mag	Spectral Type	V_r (km/s)
ι Psc	222368	23h 40m 48.0s	+05°42' 57"	J2016.5	4.13	F7 V	$+5.3 \pm 0.2$
α Cas	3712	00h 41m 27.2s	+56°37' 39"	J2016.5	2.23	K0~IIIa	-3.9 ± 0.1
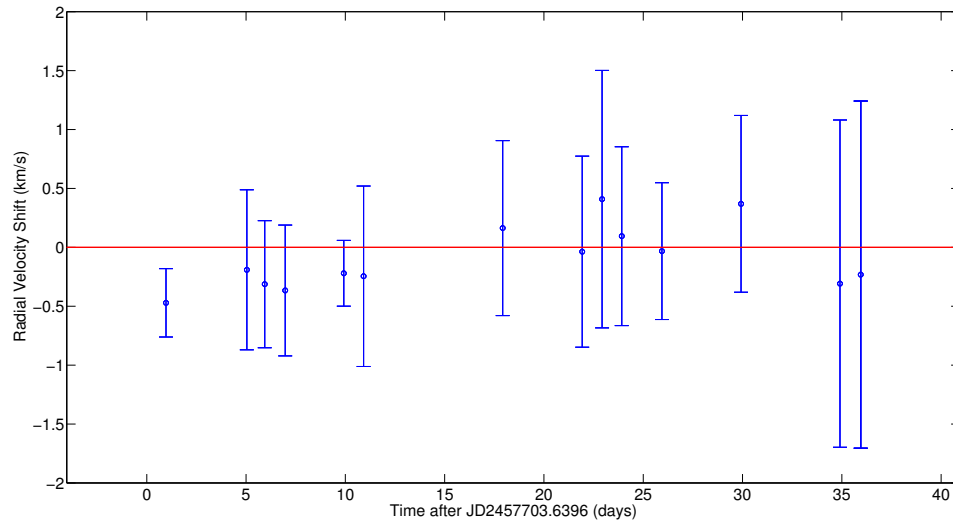
(a) Cross correlation of spectrum of α Cas taken on November 11, 2016 with α Cas spectra taken on all other nights of observation.
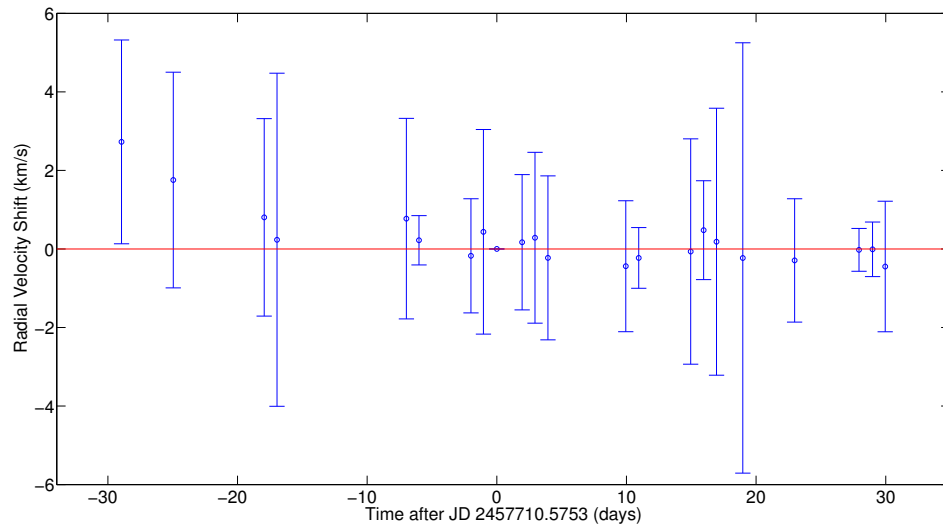
(b) Cross correlation of spectrum of ι Psc taken on November 18, 2016 with ι Psc spectra taken on all other nights of observation.

Figure 3.1: Cross correlation of radial velocity standards showing stability of the spectrograph throughout the observing run.

Table 3.2: Stellar properties of the spectroscopic binary stars observed.

Name	HD No.	α	δ	Epoch	V Mag	Spectral Type
HR 8257	205539	21h 35m 19.12s	+28°11' 51.4"	J2000.0	6.25	F0 V / F2 V
ι Peg	210027	22h 07m 00.67s	+25°20' 42.4"	J2000.0	3.76	F5 V / G8 V (est.)
ζ And	4502	00h 47m 20.32s	+24°16' 01.8"	J2000.0	4.06	K1 III

Table 3.3: The orbital parameters of the spectroscopic binary stars observed, given by Fekel et al. [2009], Fekel and Tomkin [1983], and Kővári et al. [2007].

	HD 205539	ι Peg	ζ And
P (days)	12.213446	10.213	17.7674
K1 (km/s)	52.059	48.1	25.26
K2 (km/s)	58.835	77.9	N/A
γ (km/s)	-43.003	-5.5	-24.38
ω	44.71	N/A	77
e	0.28974	0	0.013

the standard alpha Cassiopeiae (α Cas, or Schedar) was used. Its 2.24 magnitude brightness significantly reduced the exposure time needed and allowed for more observations to be taken. Typically, α Cas was observed with three 100 second exposures, which progressed to three 60 second exposures as it was discovered that modifying the star-tracking tool's input in Maxim DL increased the counts of all observations. For the F-type stars ι Peg and HD 205539, the standard iota Piscium (ι Psc) was used. This star was observed with three 400 sec exposures due to its 4th magnitude brightness.

3.1.2 Spectroscopic Binaries

The spectroscopic binary stars that were investigated in this thesis are HD 205539, ι Peg, and ζ And. These stars represent a diversity of spectral types, eccentricities, magnitudes, and number of discernible components. These are detailed in Tables 3.2 and 3.3

HD 205539, also known as HR 8257 or HIP 106595, is an F0 star with a visual magnitude of 6.25 as described in Fekel et al. [2009]. It is a double-lined binary with the F2 companion only slightly fainter than the primary, which makes the two
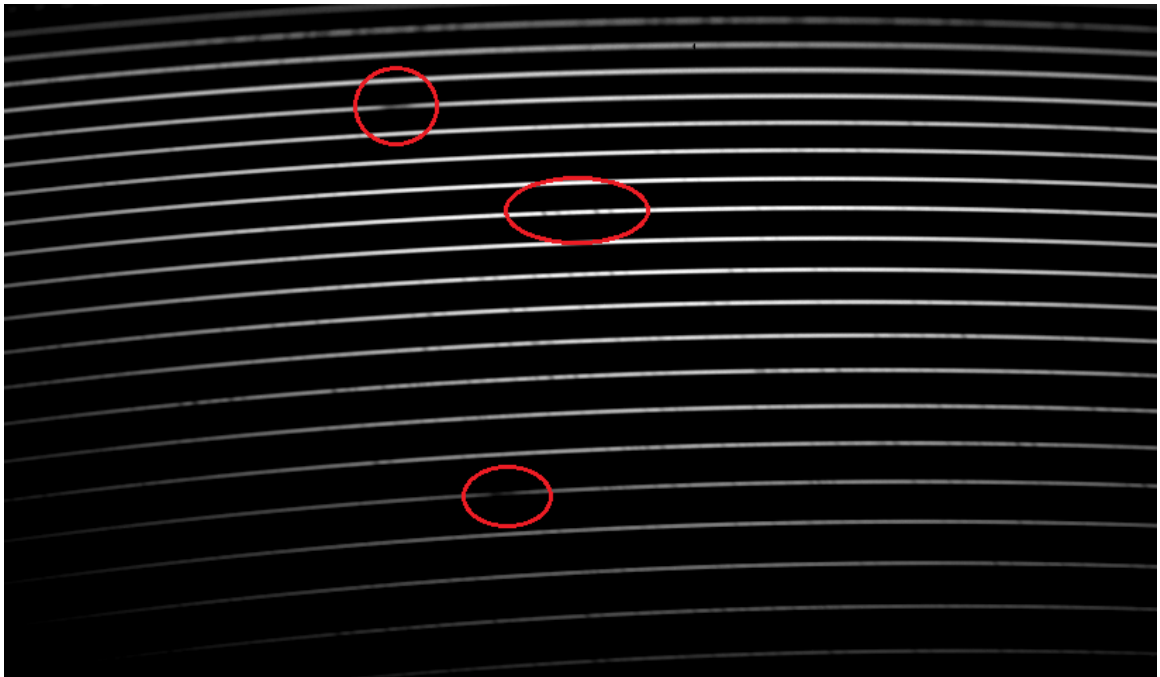
Figure 3.2: A portion of the spectrum of HD 205539 taken on November 11, 2016. The circled spectral lines, from top to bottom, are Hα, Sodium D-lines, and Hβ of the two components of the system.

sets of lines very visible in the spectrum, as shown in Figure 3.2. Its eccentricity is considerable, at nearly 0.3, which makes its argument of periastron an important parameter, described in further detail in Chapter 4.

ι Peg, also known as HD 210027 or HIP 109176 is an F5V star with a visual magnitude of 3.76 as described in Fekel and Tomkin [1983]. It is also a double-lined system, with a faint companion of possibly G5 or later spectral type. The companion is hard to detect, so there is greater error in the determination of its radial velocity. The system's eccentricity is very near 0, meaning the calculation of the argument of periastron is highly uncertain and not significant.

ζ And, also known as HD 4502 or HIP 3693 is a K1III star with a visual magnitude of 4.06 Ducati [2002]. It is a single-lined system as the companion is too faint to detect. The system's eccentricity is also very close to 0, similar to ι Peg, as shown by Kővári et al. [2007]

3.2 Typical Observing Run

Every night of observation, after the spectrograph and cameras were turned on, the AudeLA software was launched and connected to the SBIG camera and spectrograph. Once connected and turned on, the camera was cooled to its -35°C operating temperature. Simultaneously, the telescope and dome were being opened using the TCS software on the telescope control computer, as well as linking the telescope to The Sky 6 software, which controls its pointing.

After the SBIG camera was cooled, three 15-second LED/Tungsten lamp exposures were taken, followed by five 30-second Th-Ar frames. These times were determined as the longest exposure times before saturating the detector. As this was happening, the guider camera on the FIGU was connected to the Maxim DL software.

Once all of the equipment was set up and the calibration frames were taken, the telescope was slewed to the first target star, which for most nights was HD 205539. Five 30-second Th-Ar calibration frames were taken between all targets to account for any variability in the location of the Th-Ar lines on the imaging camera and any instrumental drift. This process was repeated until all target stars and radial velocity

standards for that observation night were taken.

Once all target observations were taken, a calibration set of 10 bias frames and 5 dark frames for each value of exposure time taken that night were set to run overnight since they did not require the telescope to be active. The observations taken are summarized in Appendix A.

Chapter 4

DATA ANALYSIS

4.1   Data Extraction and Reduction

The AudeLA software outputs spectrographic data in the FITS format. The convenience of the software allows for automated reduction of the data. Once all the Th-Ar calibration frames, dark frames, bias frames, LED/Tungsten frames, and object data have been taken and saved to a folder, the software automatically reduces and wavelength-calibrates the frames, as well as co-adding the exposures taken of the same object while removing cosmic rays. It automatically chooses the darks, flats, and Th-Ar frames appropriate to the data set. A reduced frame of α Cas is shown in Figure 4.2.

The primary data of the processed FITS file contains the reduced échelle two-dimensional image. The next 34 extensions contain two types of data for each of the 17 extracted orders listed in Table 2.1. These contain the non-wavelength calibrated, non-normalized one-dimensional co-added data for each order followed by the normalized and wavelength-calibrated spectrum for that order. The normalization is necessary since the intensity of light drops from the center of each order to the edges, as shown in Figure 4.2, also described in Schroeder and Hilliard [1980]. This is done automatically by the software using the LED/Tungsten exposures, seen in Figure 4.1.

The wavelength-calibrated spectrum of each order was extracted into MATLAB
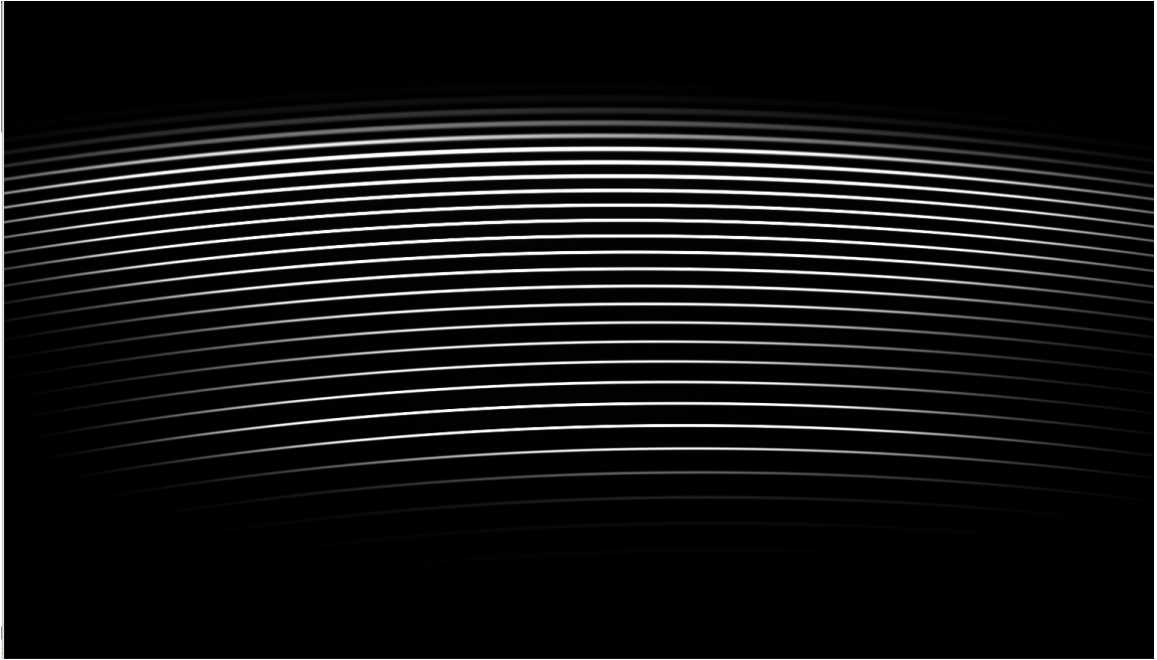
Figure 4.1: A reduced image of an LED and Tungsten lamp exposure showing all of the illuminated échelle orders.

using the *fitsread* command. The AudeLA software also stores the wavelength calibration information in the header of the appropriate section of the FITS file. This is given as a linear dispersion relation with initial wavelength of the order labeled CRVAL1 in the FITS header and the wavelength spacing labeled CDELT1.

4.2 Radial Velocity Determination

When the radial velocity of a star is calculated based on the Doppler shift of its spectral lines, the computed velocity is the total net velocity of the star towards or away from the spectrograph performing the measurement. Since this spectrograph is located at a specific point on Earth at a specific time, this calculated radial velocity is not measured from an inertial reference frame. As a result, several factors were taken into account when describing the radial velocities in this and other papers.

As a global definition, the radial velocity of a star is described as its velocity away from the Solar System barycenter. The Earth is traveling around the barycenter at
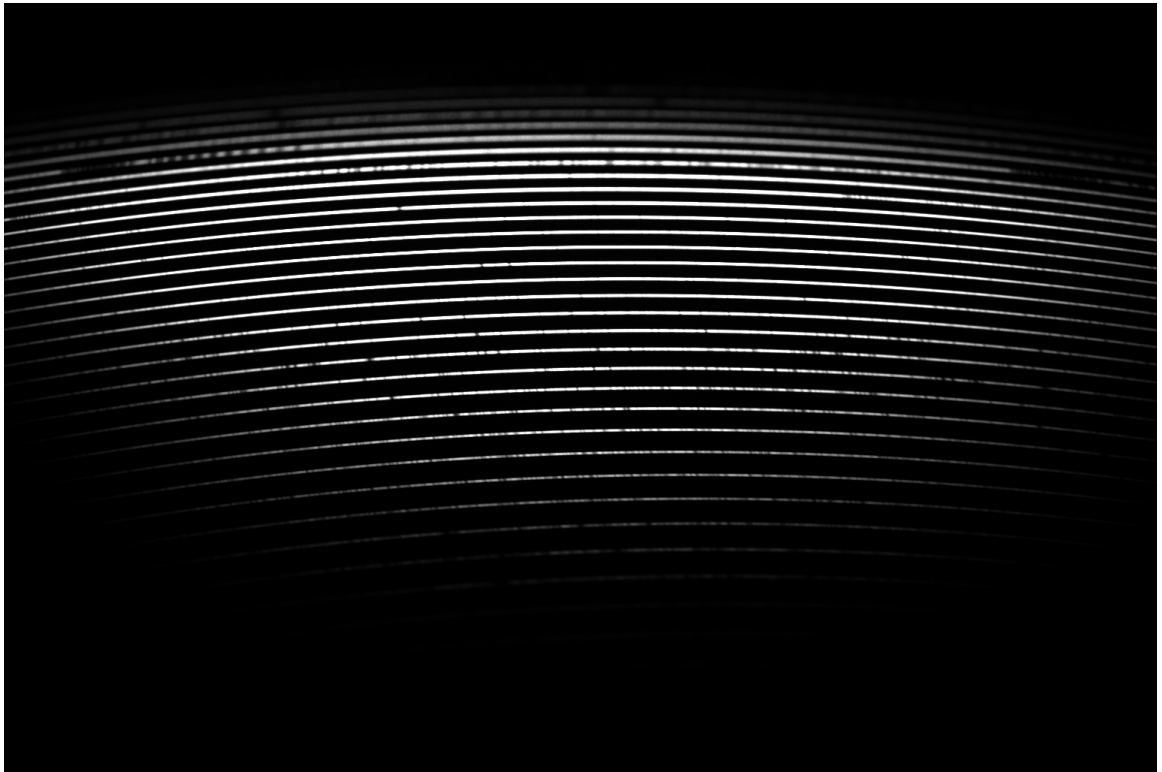
Figure 4.2: A reduced image of the spectrum of α Cas showing a full stellar spectrum as it appears on the imaging camera.
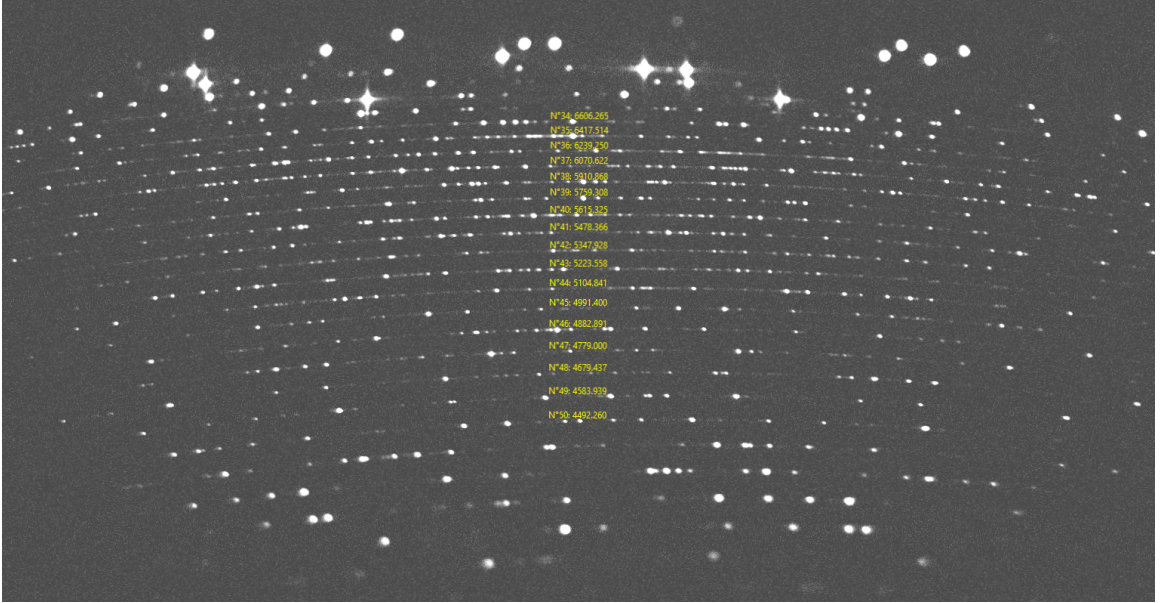
Figure 4.3: A reduced image of the Th-Ar spectrum showing the different orders of the échellogram.

approximately 30 km/s, so this velocity contribution may be significant considering we are measuring radial velocity amplitudes of 30-70 km/s. This is also a significant factor due to the fact that the shift of spectral lines was measured against a radial velocity standard star, which was not necessarily in the same location in the sky as the target star, meaning the Earth's motion toward or away from the stars is different. To compute the Earth's velocity towards a certain right ascension and declination, the following equation was used:

$$v_{Earth} = v_x \cos \delta \cos \alpha + v_y \cos \delta \sin \alpha + v_z \sin \delta \tag{4.1}$$

where v_x, v_y, and v_z are the x, y, and z components of the Earth's barycentric velocity, and α and δ are the right ascension and declination of the star. The first three values were calculated using MATLAB's *planetEphemeris* function, with the observation's Julian Date as an input, which was extracted from the FITS header.

In addition to accounting for the Earth's orbital motion, since the radial velocity of the spectroscopic binary target was calculated against a radial velocity standard,

this calculated velocity is shifted by the radial velocity of the standard. Therefore, the final result has this velocity subtracted away.

In order to determine the radial velocity of a system, the most basic concept to understand is how a spectral Doppler shift is determined. The Doppler effect tells us that a frequency shift is determined, for objects moving much slower than the speed of light, using the following equation:

$$\Delta f = \frac{v_o - v_s}{c} f_o \tag{4.2}$$

where Δf is the frequency shift due to the Doppler effect, v_o is the velocity of the observer (in our case, we set this to be 0, as we correct for observer motion), v_s is the velocity of the source, which we refer to as v_r, the radial velocity of the object, c is the speed of the wave, which in our case is the speed of light, and f_o is the original frequency of the wave.

Since our spectrograph is calibrated to measure wavelengths, we can use a basic wave relationship to convert between frequency and wavelength:

$$v = f\lambda \tag{4.3}$$

where v is the speed of the wave, f is its frequency, and λ is its wavelength.

Combining equations 4.2 and 4.3, and solving for v_r gives us:

$$v_r = c\frac{\lambda_{obs} - \lambda_o}{\lambda_o} = c\frac{\Delta\lambda}{\lambda_o} \tag{4.4}$$

where λ_{obs} is the observed wavelength of a spectral line, and λ_o is its defined rest wavelength.

Using equation 4.4, the radial velocity of a star can theoretically be calculated using any spectral line of a star if its rest wavelength can be identified. In practice, however, this is very error-ridden, depending on the width of the spectral line, which is governed by the temperature, rotation rate, and Stark broadening (Gray [1992]). This is especially true for a low-mass species such as hydrogen. As a result, finding the exact center of a spectral line and determining its shift is very impractical.
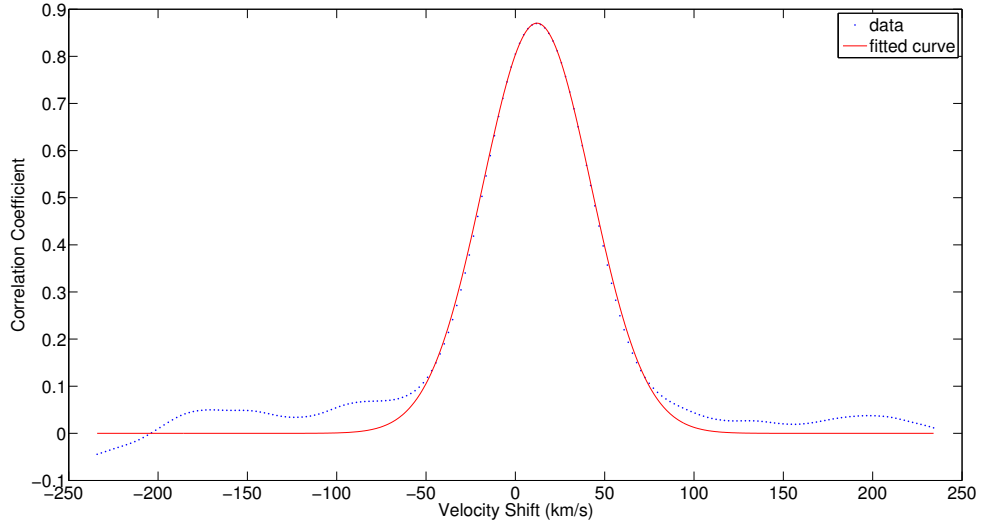
Figure 4.4: The peak of the cross-correlation coefficient curve, fitted with a Gaussian. The peak occurs at 12.1 km/s.

To solve this issue, a set of cross-correlation techniques was employed to determine the radial velocities of the stars (Hill [1993]). The equation for cross-correlation for two one-dimensional data sets is given as:

$$
c_{y_1 y_2}(k) = \begin{cases} \dfrac{1}{T} \displaystyle\sum_{t=1}^{T-k} (y_{1t} - \bar{y_1})(y_{2,t+k} - \bar{y_2}); & k = 0, 1, 2, \dots \\ \dfrac{1}{T} \displaystyle\sum_{t=1}^{T+k} (y_{1t} - \bar{y_1})(y_{2,t-k} - \bar{y_2}); & k = 0, -1, -2, \dots \end{cases} \tag{4.5}
$$

where c is the correlation coefficient, T is the maximum index of the data set, and k is the lag, or the interval by which the data sets have been shifted.

This method takes the calibrated spectral orders of each star and shifts them by a certain interval until the spectral lines have lined up. This is indicated by a peak in a graph of velocity vs. correlation coefficient, which can be seen in Figure 4.4. For a single-lined system, finding the peak of this correlation function is fairly simple, but this becomes more difficult for a double-lined system where the spectra of both stars are visible.

4.2.1 MATLAB Single-Lined Cross-Correlation

The cross-correlation process for single-lined systems was done in MATLAB using pre-existing correlation functions. Once the data for each order was obtained, a corresponding wavelength array had to be created. This was done using the dispersion relation information stored in the FITS header, which was read in using the *fitsinfo* command. This was done for both the binary star and the radial velocity standard.

The AudeLA software outputs the calibration of each order to the far edges of its visibility on the CCD. However, as can be seen in Figure 4.2, the very edges of the orders are the faintest and have the lowest signal to noise. Therefore, the first and last 5 Å of each order were trimmed to reduce noise in the data.

Once the two spectra were trimmed and wavelength arrays created, the *crosscorr* function was used to cross-correlate the spectra. A maximum lag of ±100 elements was specified which equates to about ±5 Å of shift given our dispersion relation. Once the cross correlation was done, the x-axis was converted into velocity space using equation 4.4. The resulting cross-correlation curve is shown in Figure 4.4.

Since we are only interested in the location of the peak, a Gaussian was fit to the section of the curve with a correlation coefficient greater than 0.7. While the highest point in the curve could have been used for this purpose, the spacing between each correlation point is insufficient for the resolution we desire. The Gaussian fit was created using the *fit* function and the *'gauss1'* fit in MATLAB. The location of the maximum was stored from the *coeffvalues* command.

4.2.2 TODCOR

When the same correlation technique is employed for double-lined systems, the analysis becomes much more complicated. Since there are two sets of spectra shifted in different directions, two peaks occur in the correlation curve. This phenomenon is clearly shown in Figure 4.5. While a superposition of two Gaussian curves could be used to locate the two peaks, the non-Gaussian nature of the entire correlation function makes fitting impractical and inaccurate.

To solve this issue, astronomers have developed an algorithm to determine the
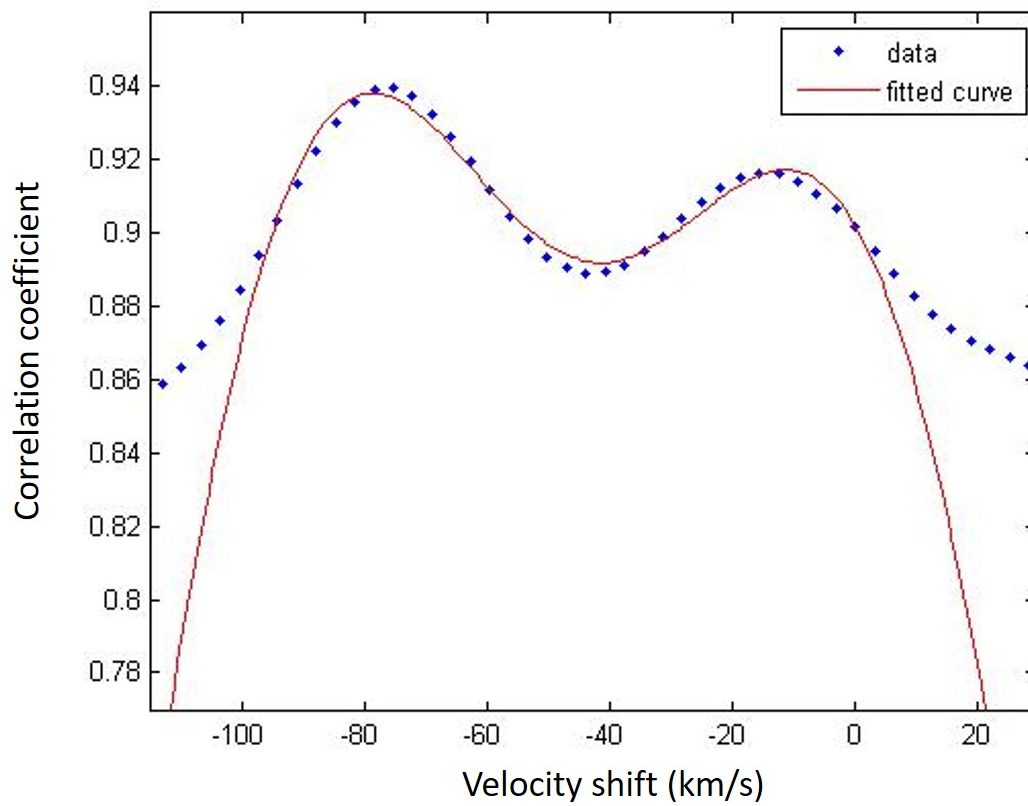
Figure 4.5: The cross correlation curve of a double-lined system. The fitted curve is comprised of two Gaussians.
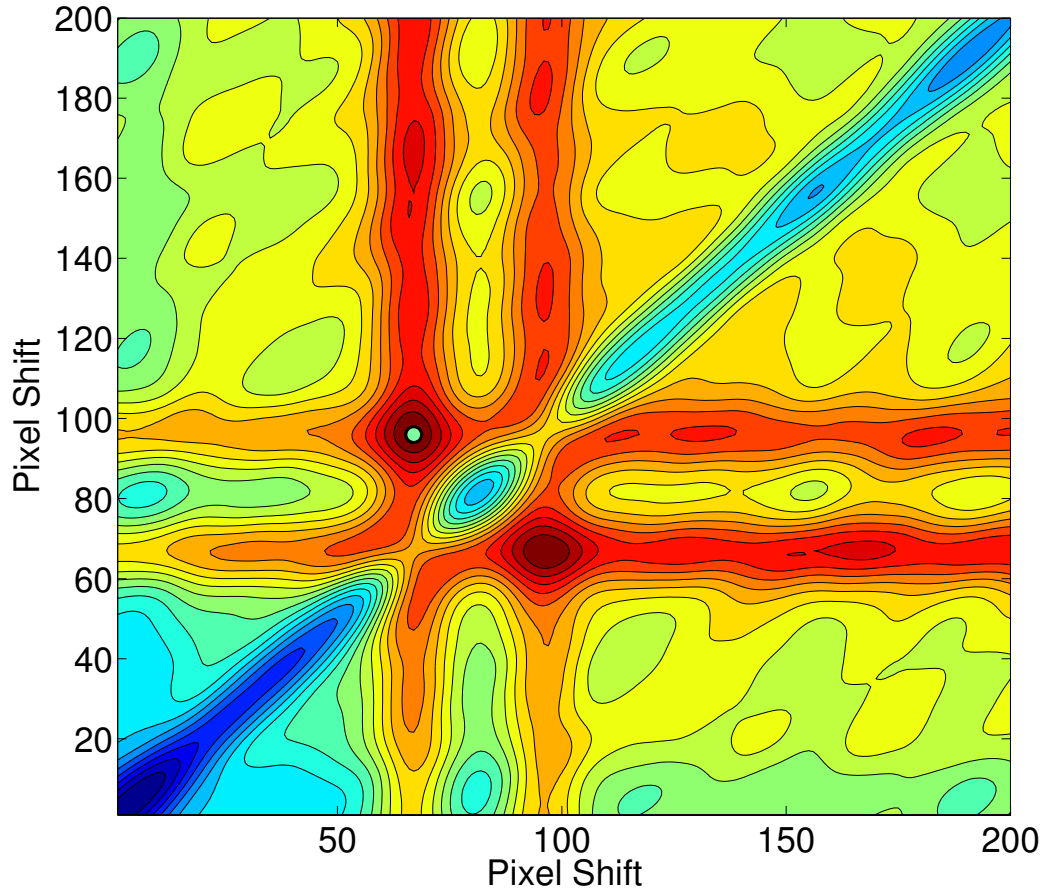
Figure 4.6: A contour plot of the matrix produced by the TODCOR function with the peak location marked by the green dot. A shift in one pixel equates to 2.6 km/s.

velocity shift of a double-lined spectroscopic binary system, called TwO-Dimensional Correlation, or TODCOR (Zucker and Mazeh [1994]).

TODCOR works by performing three cross-correlations between the target star's spectrum and model or observed spectra representing the primary and secondary stars. For this analysis, these model spectra were radial velocity standard stars listed in Table 3.1. The peak of a 2D matrix created by this algorithm is used to determine the velocity shift. A contour plot of this matrix is shown in Figure 4.6.

Written code already exists to implement the TODCOR algorithm. For this thesis,

the Interactive Data Language (IDL) code written by James Davenport (Davenport [2017]) was converted into MATLAB and used for both double-lined systems. To ensure the two codes worked identically, the same data inputs were used for both the IDL and MATLAB codes, and they were then verified to produce identical results. The MATLAB code is given in Appendix B.

4.2.3 Data Trimming

Observation Date Trimming

Once the radial velocity values and their uncertainties were determined for the primary and secondary stars for each observation date, the velocities, corrected for both the Earth's motion and the motion of the radial velocity standard, were plotted in phase space using the orbital parameters in the literature, as shown in Figure 4.8a. The phase was calculated with the simple equation:

$$Phase = (JD - T_0) \mod P \tag{4.6}$$

where JD is the Julian Date of the observation, T_0 is the epoch of periastron of the system, and P is the orbital period. This gives the decimal remainder of the number of periods that have passed since the given epoch of periastron.

Once plotted, it became fairly evident that the TODCOR algorithm had difficulty providing accurate and precise velocities for each star at the times of crossing. This is due to the heavy overlap and blending of the spectral lines when the motion of both stars is perpendicular to the line-of-sight. As a result, when determining orbital parameters, these dates were excluded to reduce error. In addition, since the secondary star for ι Peg was so faint compared to the primary, the error bars for the measurements tended to be large. As a result, any date with an error larger than 2 km/s was discarded. These velocities can be found for HD 205539, ι Peg, and ζ And in Tables 4.1, 4.2, and 4.3 respectively.

Table 4.1: Barycentric Radial Velocities found for HD 205539 after improved reduction. Starred values were not included in the orbital parameter determination due to high uncertainty between all 17 orders.

Julian Date	Primary RV (km/s)	Uncertainty (km/s)	Secondary RV (km/s)	Uncertainty (km/s)
2457680.566944	-78.4	± 0.4	0.7	± 0.7
2457681.555159	-70.9	0.3	-9.8	0.8
2457685.551699	-0.6	0.6	-90.8	0.3
2457692.561342	-80.4	0.5	0.8	0.4
2457693.556556	-72.0	0.5	-6.5	0.8
2457703.535618**	-80**	4.6**	-3**	6.8**
2457704.489128	-82.2	0.3	1.9	0.3
2457708.515765	-26.0	1.1	-51.7	0.4
2457709.469861	-10.4	0.7	-77.1	0.3
2457710.505287	10.97	0.09	-102.9	0.3
2457712.464744	-5.4	0.8	-82.3	0.4
2457713.457565	-54.0	0.4	-34.1	0.6
2457714.458098	-76.1	0.3	-4.5	0.4
2457720.460223**	-31**	2.2**	-49.7	0.9
2457721.478196**	-15	1.3	-66.4**	4.9**
2457725.468382**	-49	1.0	-33.7**	2.6**
2457726.464209**	-67.5**	4.7**	-9.4**	3.5**
2457727.457802	-82.9	0.3	5.1	0.6
2457729.490258	-78.2	0.3	-0.7	0.7
2457733.463256	-18.7	1.3	-65.4	0.5
2457738.453406	-67.4	0.3	-12	1.5
2457739.499781	-81.9	0.2	4.4	0.8
2457740.473084	-84.2	0.3	5.8	0.6

Table 4.2: Barycentric Radial Velocities found for ι Peg after improved reduction. Starred values were not included in the orbital parameter determination due to high uncertainty between all 17 orders.

Julian Date	Primary RV (km/s)	Uncertainty (km/s)	Secondary RV (km/s)	Uncertainty (km/s)
2457680.614726**	13**	± 9.1**	-6	± 1.3
2457681.609491**	-36.2	0.3	39**	3.3**
2457685.601278**	0**	12.4**	-3.7	0.3
2457692.606992**	-50.0	0.3	60**	5.0**
2457693.602177**	-51.5	0.3	64**	5.0**
2457703.581830**	-53.1	0.3	69**	3.7**
2457704.554349	-42.6	0.2	55.3	0.8
2457708.598573**	42.6	0.8	-77**	5.2**
2457709.514955	34.3	0.3	-68.0	0.7
2457710.550361	9.97	0.08	-33.61	1.0
2457712.509909**	-41.5	0.3	50**	3.5**
2457713.503096	-53.1	0.3	71.9	0.6
2457714.504365	-47.0	0.2	61.3	0.8
2457720.505879**	17.6	0.7	-39**	3.6**
2457721.461235**	-1**	7.9**	-4	1.5
2457725.513438	-30.3	0.3	33	1.9
2457726.508956**	-5**	4.2**	-5**	4.6**
2457727.507879	23.4	0.7	-54	1.2
2457729.535047**	40.3	0.4	-73**	4.9**
2457733.508136**	-50.3	0.3	61**	4.4**
2457738.497811**	38.3	0.4	-67**	5.3**
2457739.544270**	40.9	0.4	-61**	8.6**
2457740.518474	26.4	0.7	-58	1.1

Table 4.3: Barycentric Radial Velocities found for ζ And after improved reduction. No radial velocities had high enough uncertainty to be excluded from the orbital parameter determination.

Julian Date	Radial Velocity (km/s)	Uncertainty (km/s)
2457703.620897	-1.7	± 0.2
2457704.590966	1.1	0.1
2457708.661394	-1.72	0.08
2457709.561096	-25.3	0.1
2457710.593800	-34.7	0.2
2457713.543106	-49.0	0.1
2457714.539203	-47.6	0.1
2457721.544482	-1.2	0.2
2457725.547847	-9.1	0.8
2457726.545425	-18.2	0.2
2457727.541584	-27.0	0.4
2457729.569231	-42.9	0.1
2457733.533644	-43.2	0.2
2457738.532165	-3.4	0.6
2457739.577638	0.0	0.3
2457740.552352	1.2	0.3

4.3   Orbital Parameter Determination

4.3.1   Spectroscopic Binary Systems' Orbital Parameters

A binary star system is described with a set of 10 orbital parameters. These parameters, combined with Kepler's third law, can be used to determine the mass of each individual star (Batten [1973]). Some of these parameters are shown in Figure 4.7. The full list of parameters is as follows:

- P, the orbital period of the system, or the time it takes for the stars to complete one orbit around the center of mass. This is given in decimal days.

- i, the inclination of the orbital plane, defined as the angle between the orbital plane and the plane of the celestial sphere. This is given in degrees.

- Ω, the position angle of the ascending node, defined as the angle, measured from north to east on the celestial plane, to the line of the ascending node, or the point at which the star crosses the plane of the sky while moving away from the Earth. This is given in degrees.

- ω, the argument of periastron, defined as the angle between the ascending node and the point of periastron, where the two stars are closest together, measured in the plane of the orbit. For a binary system, this is considered for the primary component. The secondary component has an argument of periastron exactly equal to this value plus 180. This is given in degrees.

- a, the semi-major axis of the orbit, half of the distance between periastron and apoastron, the closest and farthest distances between the stars in the orbit. For binary stars, this is split into two, a_1 and a_2, one for each star. This is given in Astronomical Units (AU) or km.

- e, the eccentricity of the orbit. This value is unitless.

- T_0, the time of periastron. This is the time that the stars are passing through periastron. This is given as a Julian Date.

Figure 75. Orbital ellipse in true plane.
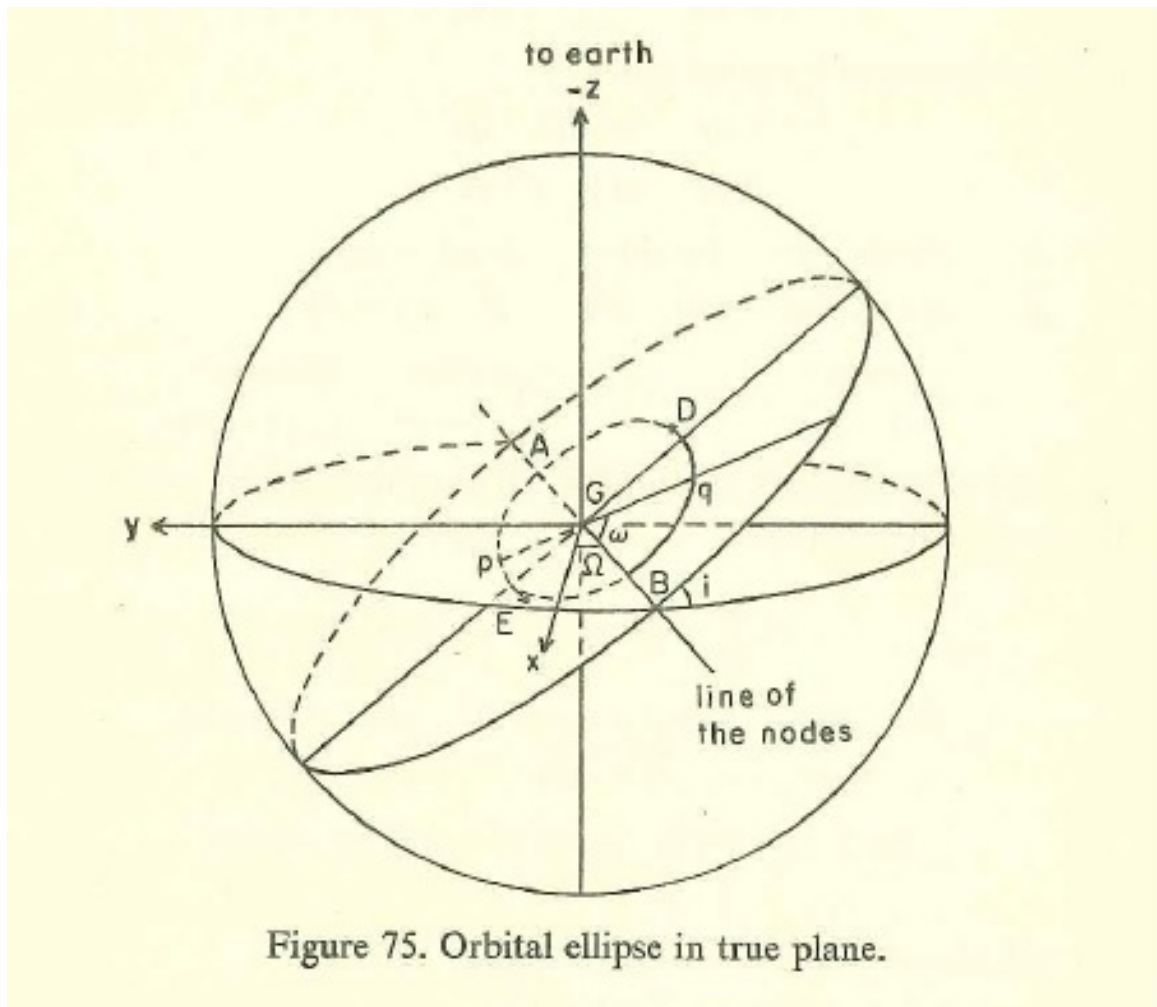
Figure 4.7: A diagram showing the orbital parameters in a 3D space (Binnendijk [1960]).

- γ, the radial velocity of the center of mass of the binary system. This is given in km/s.

- K_1, the radial velocity semi-amplitude of the primary star. This is given in km/s.

- K_2, the radial velocity semi-amplitude of the primary star. This is given in km/s.

Due to the lack of inclination data for non-eclipsing and non-visual binaries, the quantities Ω, i, and a are not capable of being directly calculated. However, the quantities $a_1 \sin i$ and $a_2 \sin i$ can be calculated. From an expression for the radial motion of an ellipse, it can be shown that:

$$K = \frac{2\pi a \sin i}{P\sqrt{1 - e^2}} \tag{4.7}$$

The derivation for this formula can be found in Binnendijk [1960]. If K is given in km/s and P is given in days, this formula can be rearranged to solve for $a \sin i$, which will be given in km. This formula is as follows:

$$a \sin i = 13,751 K P \sqrt{1 - e^2} \tag{4.8}$$

Since Ω, i, and a are not measured for non-eclipsing and non-visual systems, the parameters that can be found for spectroscopic systems are P, T_0, e, K_1, γ, and ω. For double-lined systems, K_2 can be found as well. The relationship between all these values and the radial velocities previously calculated can be found using the following:

$$V_r = V_o + Ke\cos\omega + K\cos(v + \omega) \tag{4.9}$$

where v is the true anomaly of the system, which is calculated using the *Kepler* MATLAB code provided in Appendix B.

4.3.2 Initial Orbital Element Comparison

Equation 4.9 was used to create all the theoretical radial velocity curves for the spectroscopic binaries, which allowed comparison between the radial velocity data taken and the theoretical orbit based on the orbital parameters. The orbital elements provided in previous studies were used as an initial comparison. The *orbitplot.m* MATLAB code was written for creating a theoretical curve, as well as for calculating the theoretical radial velocity at a given observation time.

4.3.3 Spectroscopic Binary Solver

In order to solve for the orbital parameters given the radial velocity data, the Spectroscopic Binary Solver (SBS) software developed by Johnson [2004] was used. Text files containing the Julian Dates of the observations, the calculated radial velocities, and the uncertainties were fed into the software. After this, the software automatically determined the orbital parameters, along with the uncertainties. This is done using the Downhill Simplex method, and is described further in Johnson [2004].

4.3.4 Spectrograph Reduction Analysis

On December 18, 2016, while reducing the spectra of the previous night, a complete erasure of the stored AudeLA setup occurred. While the setup was being recovered through previous saved analysis, it was discovered that the spectrograph reduction until that night was using an α of 63.0°as opposed to the ideal 62.7°. As a result, the previously reduced data was now in doubt with regards to accuracy. Therefore, all previously reduced data was reduced again with the ideal α value, which minimized the deviation between the AudeLA software's prediction of the location of Th-Ar lines and their true location, allowing for a more reliable wavelength calibration. This slightly changed the radial velocities calculated for each date, which also affected the orbital parameters found by the SBS software. While not a significant change, the new reduction caused most of the derived quantities to move closer to the literature values, signifying that it is important to use the correct AudeLA inputs when doing radial velocity analysis.

4.3.5 Orbital Parameter Results

Once the SBS software analyzed the input radial velocity data, radial velocity curves were created to check that the SBS software reliably fit the data. The phased plots for the three binary systems using the parameters given by the SBS are shown in Figures 4.8, 4.9, and 4.10. As can be seen, the velocity data fits the curves very well, and the observed-calculated (O-C) plots show the difference in the data versus the theoretical curves to be very close to zero, signifying a good fit.

The SBS orbital parameters were then compared with the literature. The parameters for all three stars with the exception of the T_0 values are shown side by side with the parameters from the literature in Tables 4.4, 4.5, and 4.6. The T_0 values for the three stars are JD 2457675.57 ± 0.04, JD 2457672.0 ± 0.8, and JD 2457693.5 ± 1.4 for HD 205539, ι Peg, and ζ And, respectively. In addition, these comparisons are shown graphically in Figures 4.11 to 4.16. As is evident from these figures, the orbital parameters from this analysis agree with previously published values to within two standard deviations.

Table 4.4: HD 205539 Orbital Parameter Comparison with Literature.

Parameter	SBS value	Fekel et al. [2009]	Difference
Period (days)	12.195 ±0.008	12.21345 ±0.00001	-0.01845 ±0.00801
γ (km/s)	-42.2 ±0.2	-43.001 ±0.023	0.801 ±0.223
K1 (km/s)	52.7 ±0.5	52.054 ±0.038	0.646 ±0.538
K2 (km/s)	61.5 ±0.6	58.829 ±0.061	2.671 ±0.661
e	0.295 ±0.007	0.28953 ±0.00057	0.00547 ±0.00757
ω (degrees)	44.9 ±1.2	44.79 ±0.12	0.11 ±1.32

Table 4.5: ι Peg Orbital Parameter Comparison with Literature.

	SBS parameters	Fekel and Tomkin [1983]	Difference
Period (days)	10.202 ±0.005	10.21303 ±0.000013	-0.01103 ±0.005013
γ (km/s)	-5.4 ±0.2	-5.5 ±0.2	0.1 ±0.4
K1 (km/s)	47.7 ±0.2	48.1 ±0.2	-0.4 ±0.4
K2 (km/s)	77.0 ±0.4	77.9 ±0.3	-0.9 ±0.7
e	0.008 ±0.004	0 ±0	0.008 ±0.004

Table 4.6: ζ And Orbital Parameter Comparison with Literature.

	SBS parameters	Kővári et al. [2007]	Difference
Period (days)	17.78	17.7674	0.0126
	±0.03	±0.0048	±0.0348
γ (km/s)	-23.6	-24.38	0.78
	±0.1	±0.21	±0.31
K1 (km/s)	25.2	25.26	-0.06
	±0.1	±0.31	±0.41
e	0.017	0.013	0.004
	±0.007	±0.011	±0.018
ω (degrees)	128	77	51
	±35	±52	±87
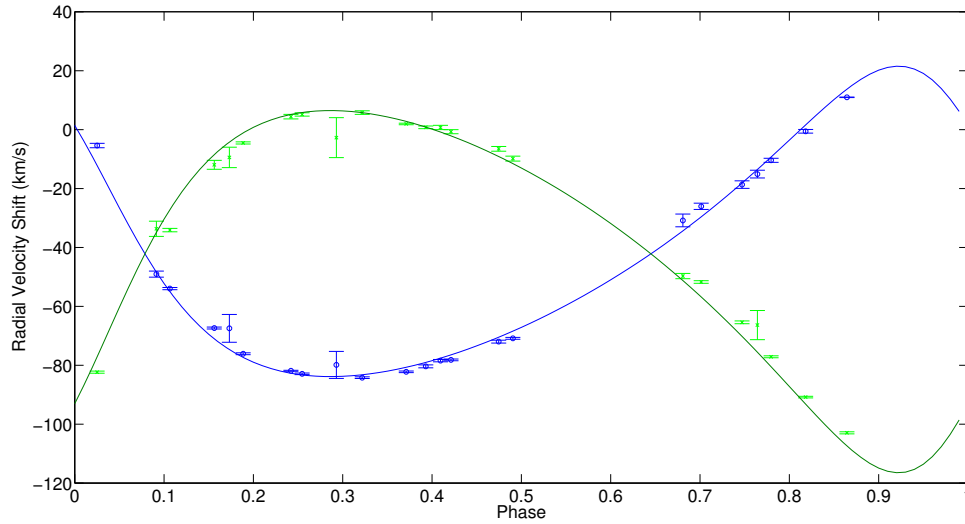
(a) HD 205539 Radial Velocity Curve
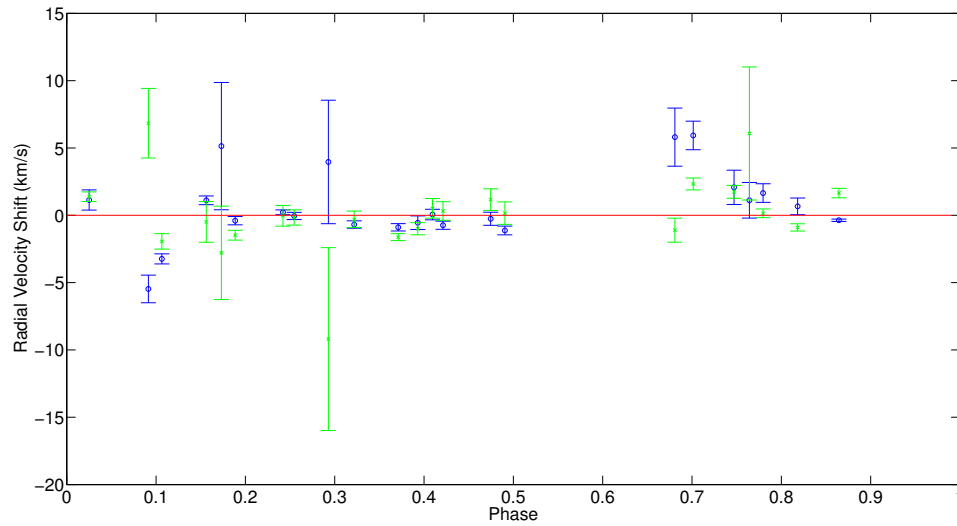
(b) HD 205539 O-C Plot

Figure 4.8: Comparison between RV data and theoretical curves produced using SBS orbital parameters for HD 205539.
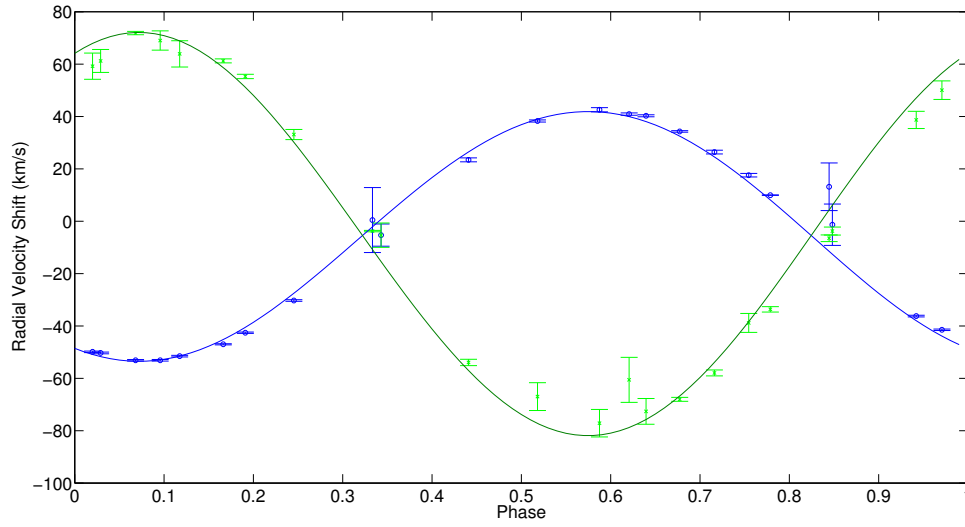
(a) ι Peg Radial Velocity Curve
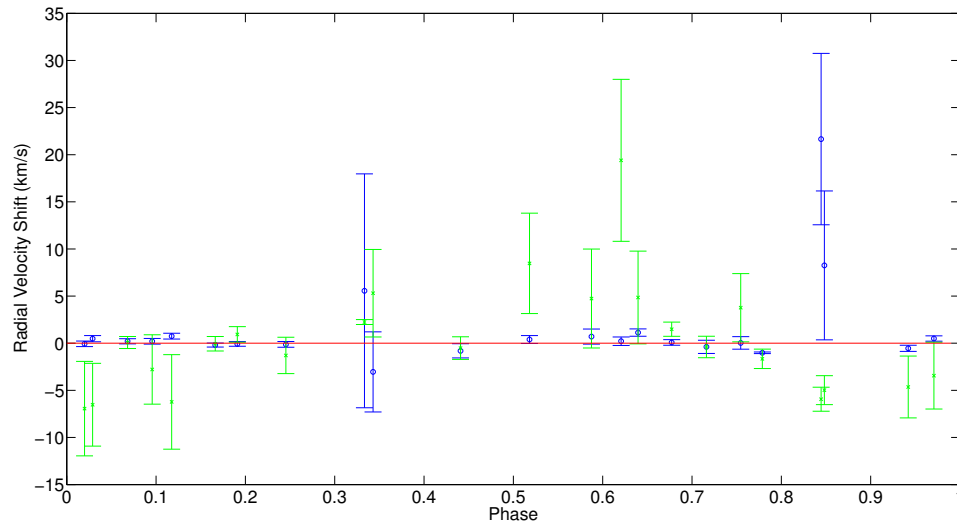
(b) ι Peg O-C Plot

Figure 4.9: Comparison between RV data and theoretical curves produced using SBS orbital parameters for ι Peg.
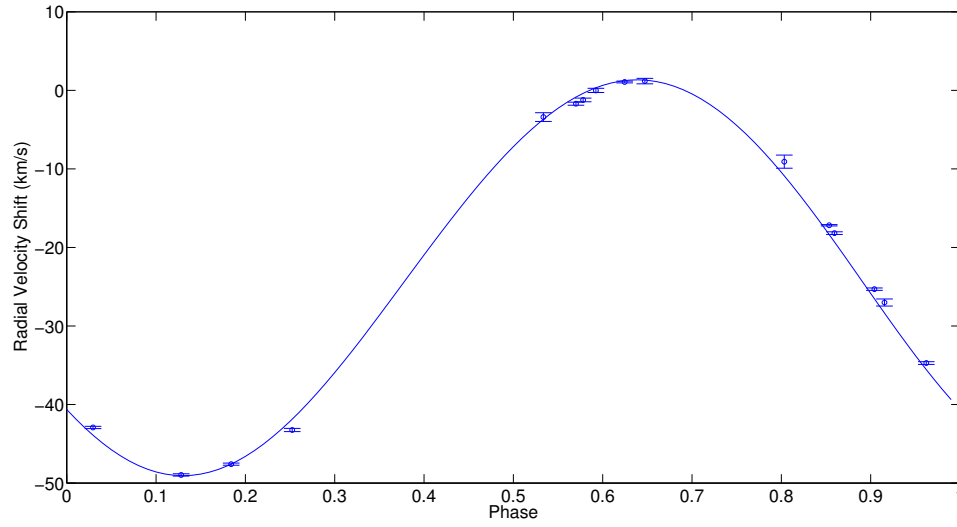
(a) ζ And Radial Velocity Curve
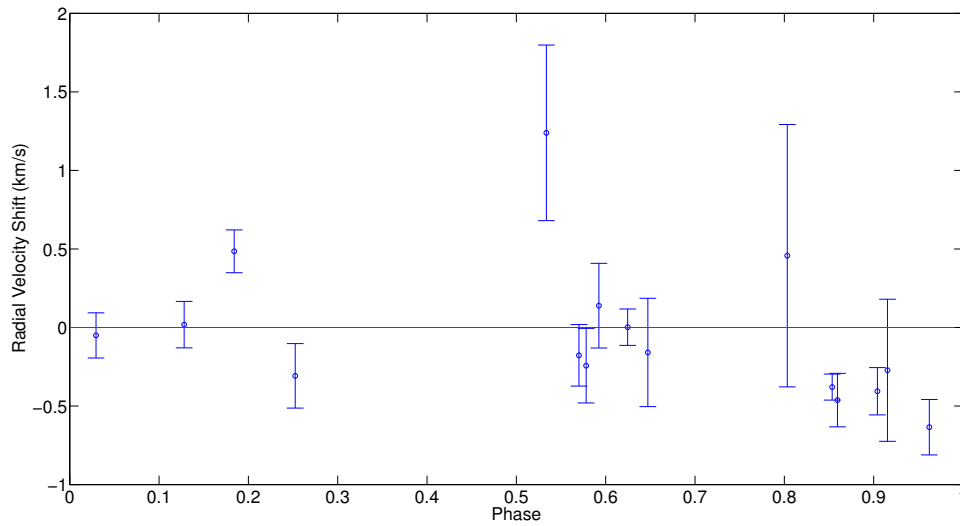
(b) ζ And O-C Plot

Figure 4.10: Comparison between RV data and theoretical curves produced using SBS orbital parameters for ζ And.
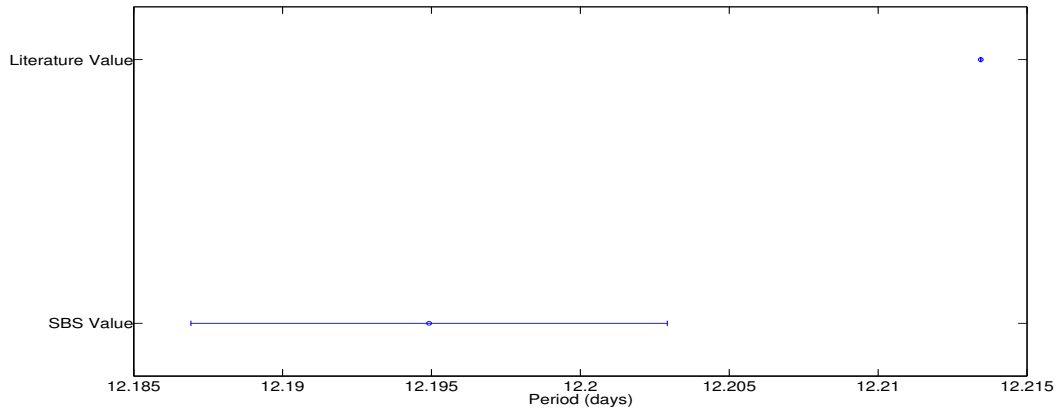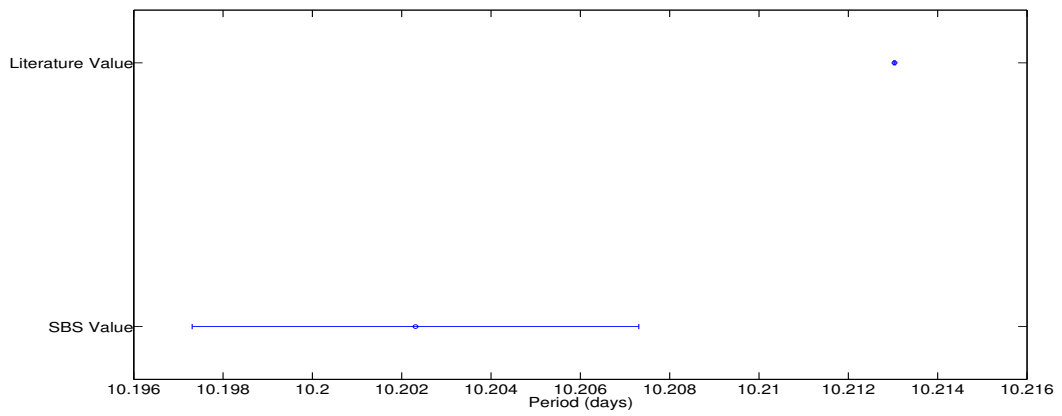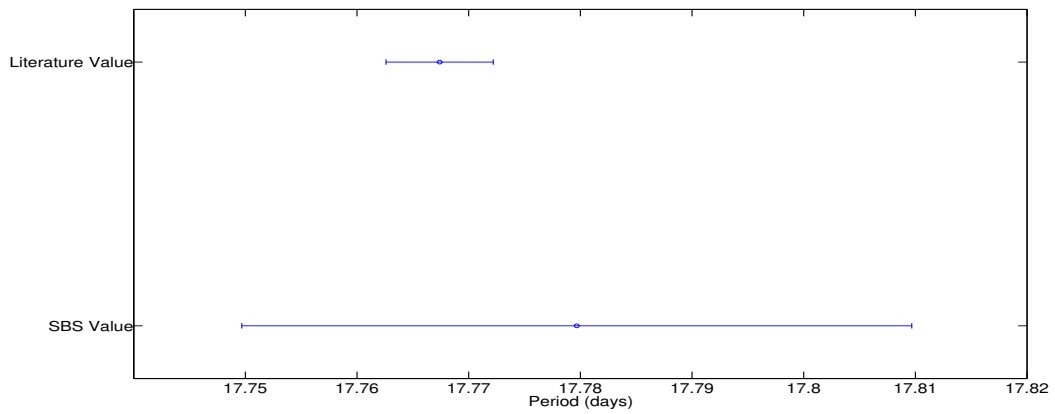
(a) HD 205539

(b) ι Peg

(c) ζ And

Figure 4.11: Comparison between orbital periods found by the SBS software and previous literature values for all three spectroscopic binaries.
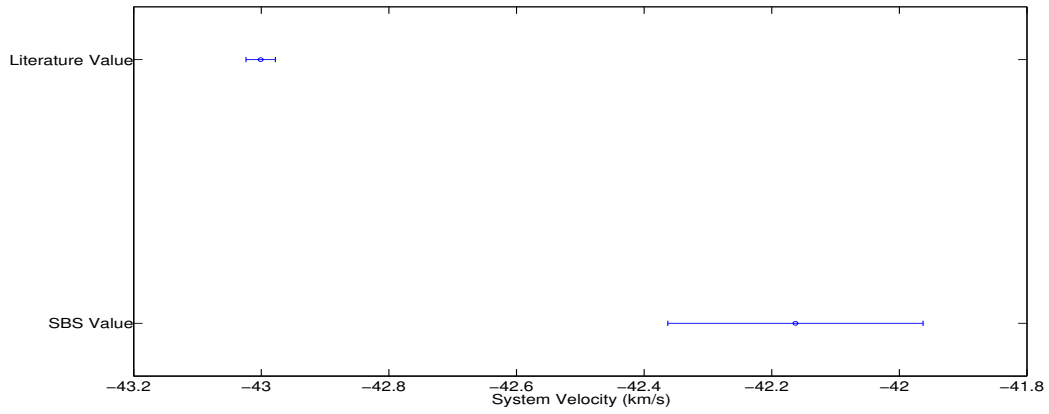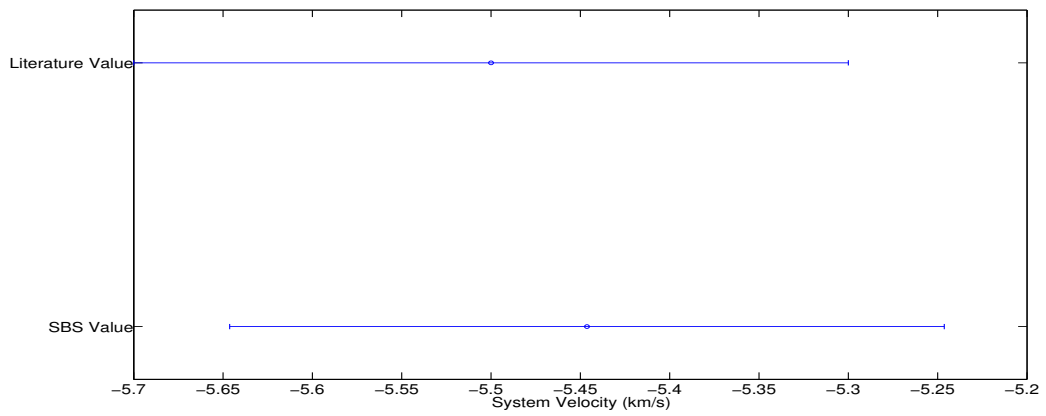
(a) HD 205539

(b) ι Peg
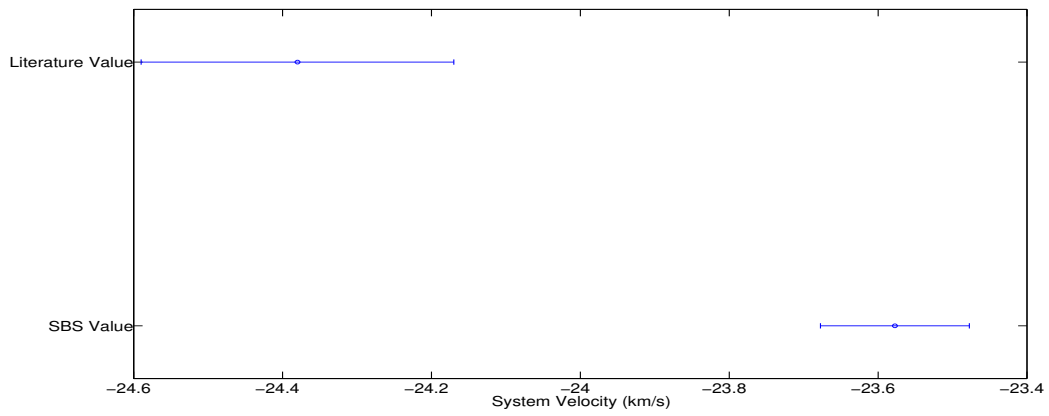
(c) ζ And

Figure 4.12: Comparison between γ values found by the SBS software and previous literature values for all three spectroscopic binaries.

(a) HD 205539

(b) ι Peg
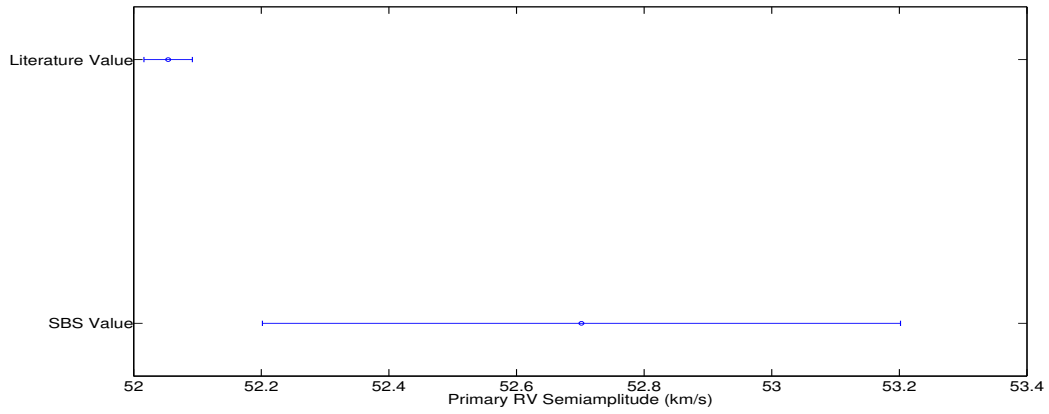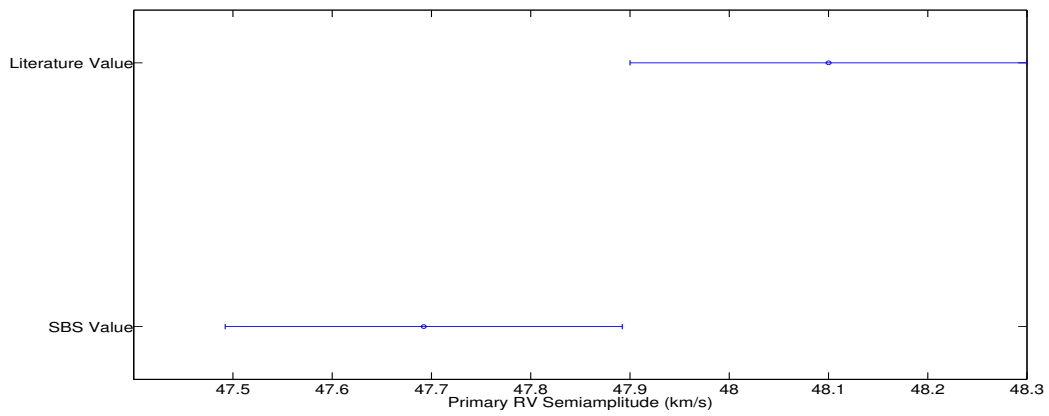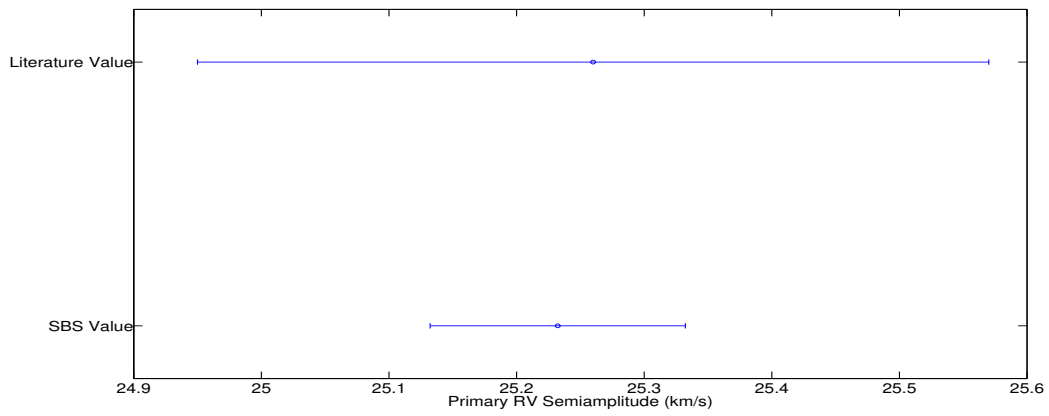
(c) ζ And

Figure 4.13: Comparison between K1 values found by the SBS software and previous literature values for all three spectroscopic binaries.
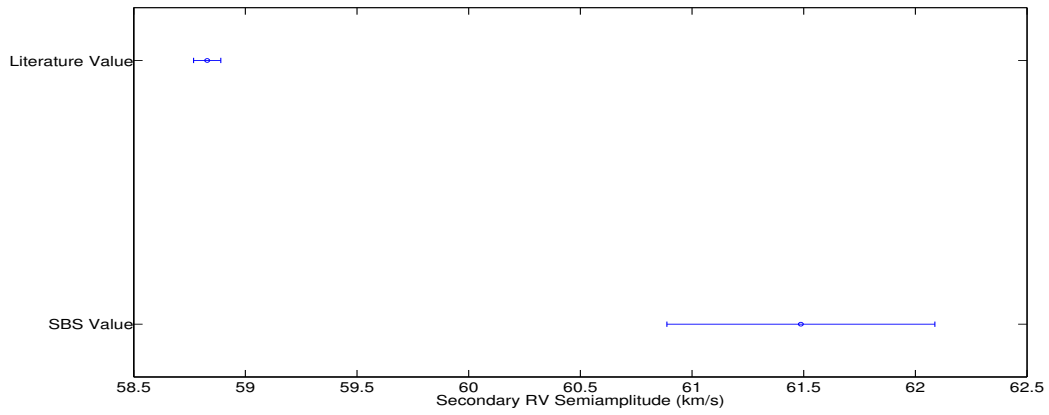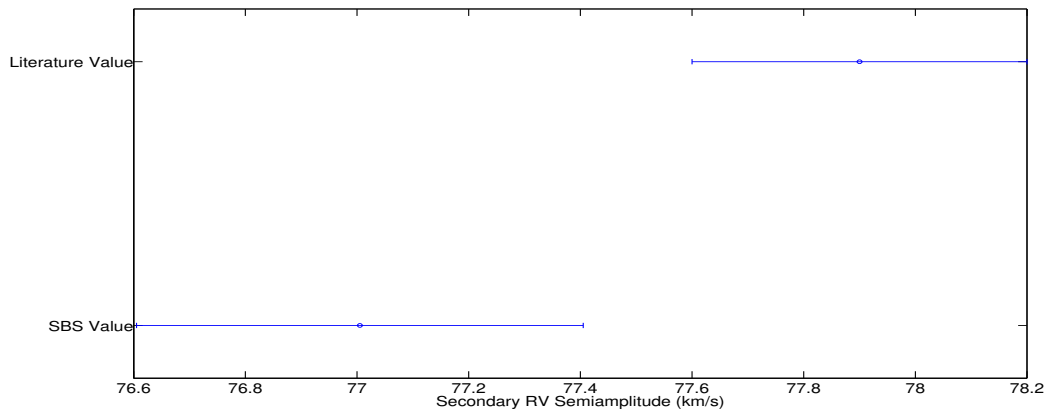
(a) HD 205539

(b) ι Peg

Figure 4.14: Comparison between K2 values found by the SBS software and previous literature values for all three spectroscopic binaries.

(a) HD 205539

(b) ι Peg
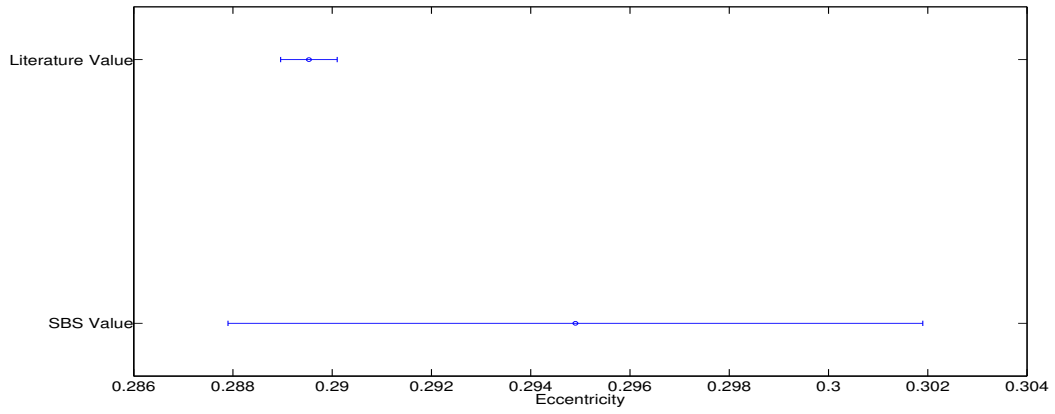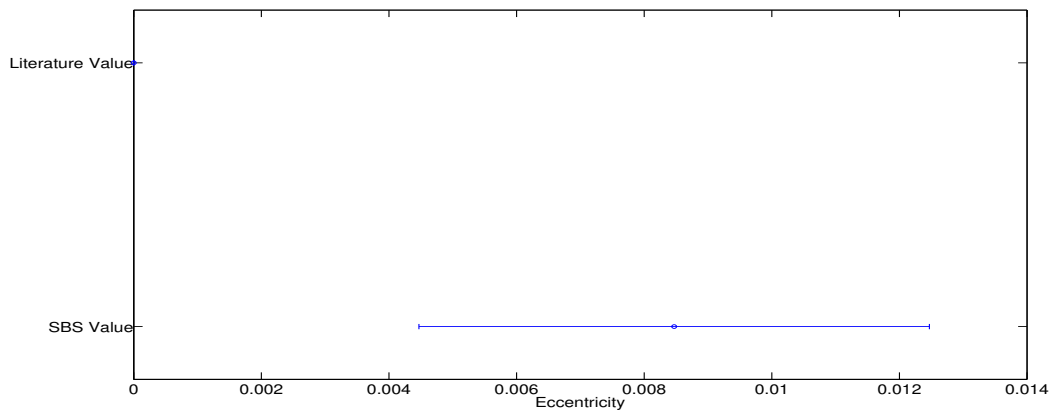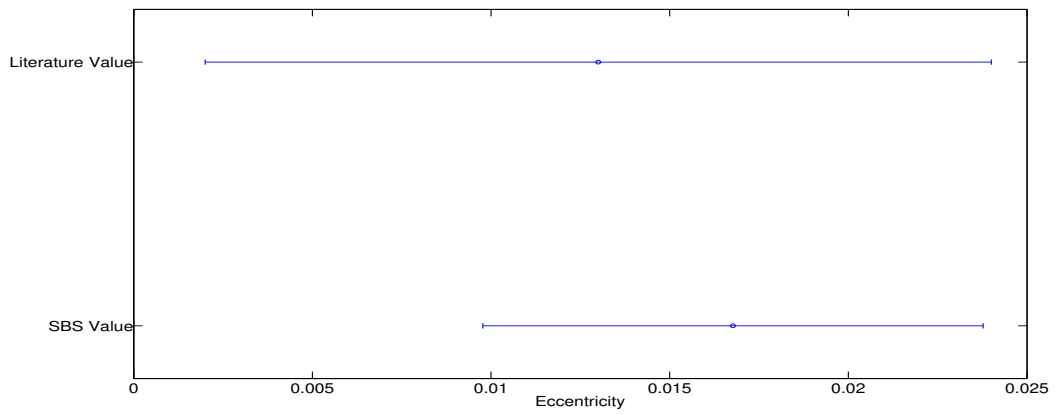
(c) ζ And

Figure 4.15: Comparison between eccentricity values found by the SBS software and previous literature values for all three spectroscopic binaries.
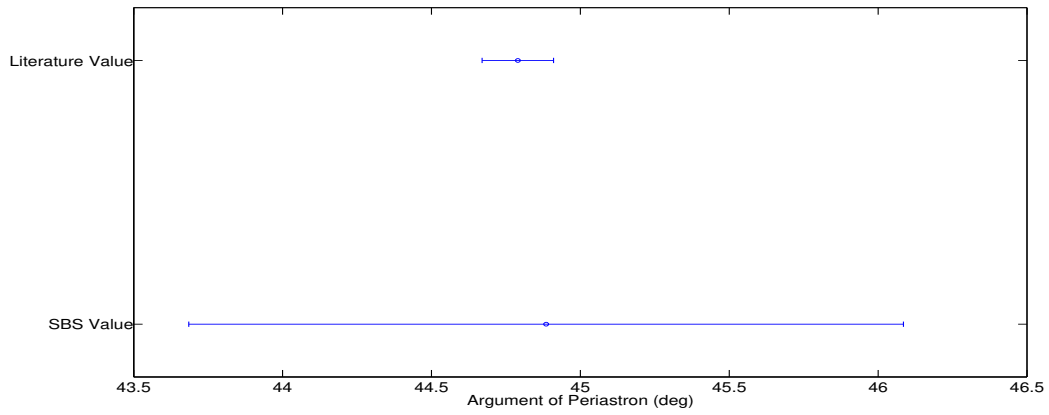
(a) HD 205539
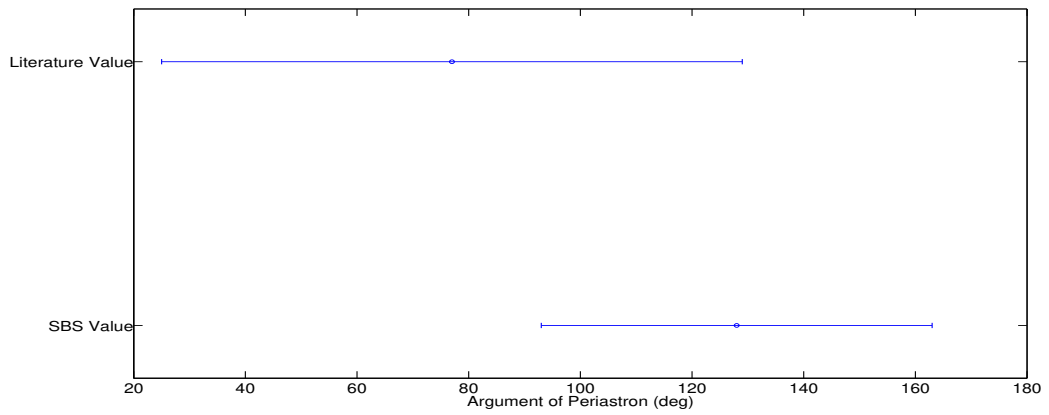
(b) ζ And

Figure 4.16: Comparison between ω values found by the SBS software and previous literature values for all three spectroscopic binaries.

Chapter 5

CONCLUSIONS AND FUTURE WORK

In this thesis, the ability to reproduce previous spectroscopic binary studies was examined. Through obtaining the orbital parameters of spectroscopic binary stars, information about their stellar masses can be obtained, which is critical in understanding stellar evolution and composition.

In order to determine these orbital parameters, a series of 25 nights of radial velocity data was taken of three previously-investigated spectroscopic binary systems, HD 205539, ι Psc, and ζ And. These stars were chosen due to their variety in spectral type, magnitude, eccentricity, and number of visible components. Looking at these stars showed that stars as early as F spectral type can be analyzed with good accuracy and precision. In addition, stars with faint but visible secondary components can be analyzed, shown by the ι Psc analysis. Looking at ζ And shows that single-lined systems can be analyzed as well.

All observations were taken at Embry-Riddle Aeronautical University with the 1-meter telescope on the roof of the College of Arts and Sciences Building combined with a fiber-fed échelle spectrograph. All data was reduced and wavelength-calibrated using the AudeLA software provided by Shelyak Instruments. The radial velocities were obtained using cross-correlation methods using built-in MATLAB code and a MATLAB conversion of the TODCOR algorithm (Zucker and Mazeh [1994]) written

by James Davenport (Davenport [2017]). With all 17 échelle orders from 34 to 50 analyzed, a radial velocity precision of approximately 1 km/s was achieved, better than the 25 km/s given with an R of 12,000.

The orbital parameters of the stars were found using the SBS software created by Delwin Johnson (Johnson [2004]). These calculated parameters were compared with the solutions given in Fekel et al. [2009] for HD 205539, Fekel and Tomkin [1983] for ι Peg, and Massarotti et al. [2008] for ζ And. The parameters found with SBS agreed with the literature to a few percent, and within two standard deviations.

Future work can be done to improve the analysis of spectroscopic binaries begun by this thesis. Instead of using radial velocity standards, model stellar spectra can be used to cross-correlate against, which may provide higher accuracy. In addition to this, more thorough analysis can be done to improve the filtering of the orders. Each order can be looked at individually to determine what spectral lines occur and whether the Telluric spectrum may have a significant effect on the cross-correlation.

From these results, it can be concluded that the software pipeline developed for analyzing spectroscopic binary stars through the ERAU 1-meter and échelle spectrograph can produce accurate and precise orbital solutions, and can be applied to binary star orbits that do not have well-defined orbital parameters. By looking at these grade 3 or lower stars, improvements to their determined orbital elements will have a significant scientific impact on our understanding of stellar composition and evolution.

Chapter 6

APPENDIX A - OBSERVATION SUMMARY

Table 6.1: List of all observations taken.

Date	Star Name or Exposure Type	Num. of Exposures	Exposure Time (s)	Comments
10/18/2016	β Aqr	3	400	Almost saturating
	HAT-P-2	1	1800	Test for exoplanet
	Th-Ar	5	30	
	HD205539	3	1200	
	ι Peg	3	400	
	Th-Ar	5	30	
	ι Psc	3	400	
	Th-Ar	5	30	
10/19/2016	β Aqr	3	150	300s saturates
	Th-Ar	5	30	
	HD205539	3	1200	
	ι Peg	3	400	
	Th-Ar	5	30	
Continued on next page				

Table 6.1: List of all observations taken.

Date	Star Name or Exposure Type	Num. of Exposures	Exposure Time (s)	Comments
	ι Psc	3	400	
10/23/2016	β Aqr	3	150	
	HAT-P-2	3	1200	
	Th-Ar	5	30	
	ι Peg	3	400	
	Th-Ar	5	30	
	ι Psc	3	400	
10/30/2016	35 Peg	3	400	
	Th-Ar	5	30	
	HD 205539	3	1200	
	Th-Ar	5	30	
	ι Peg	3	400	
	Th-Ar	5	30	
	ι Psc	3	400	
10/31/2016	35 Peg	3	400	
	Th-Ar	5	30	
	HD 205539	3	1200	
	Th-Ar	5	30	
	ι Peg	3	400	
	Th-Ar	5	30	
	ι Psc	3	400	
11/10/2016	Th-Ar	5	30	
	35 Peg	3	400	
	HD 205539	3	1200	
	Th-Ar	5	30	
	ι Peg	3	400	
Continued on next page				

Table 6.1: List of all observations taken.

Date	Star Name or Exposure Type	Num. of Exposures	Exposure Time (s)	Comments
	Th-Ar	5	30	
	ι Psc	3	400	
	Th-Ar	5	30	
	ζ And	3	400	
	Th-Ar	5	30	
	α Cas	3	100	
11/11/2016	HD 205539	3	1200	
	Th-Ar	5	30	
	35 Peg	3	400	
	Th-Ar	5	30	
	ι Peg	3	400	
	Th-Ar	5	30	
	ι Psc	3	400	
	ζ And	3	400	
	Th-Ar	5	30	
	α Cas	3	100	
	Th-Ar	5	30	
	υ Peg	3	400	
	Th-Ar	5	30	
	υ And	3	400	
	α Tri	2	400	Cloudy during 2nd exposure
11/12/2016	HD 205539	3	1200	
	Th-Ar	5	30	
	ι Psc	3	400	
	Th-Ar	5	30	
Continued on next page				

Table 6.1: List of all observations taken.

Date	Star Name or Exposure Type	Num. of Exposures	Exposure Time (s)	Comments
	ι Peg	2	400	Too humid to continue
11/15/2016	Th-Ar	5	30	
	HD 205539	3	1200	
	Th-Ar	5	30	
	ϵ Cep	3	400	
	Th-Ar	5	30	
	ι Psc	3	400	
	Th-Ar	5	30	
	ι Peg	2	400	
	Th-Ar	5	30	
	HR 8765	3	1200	
	Th-Ar	5	30	
	ζ And	3	400	
	Th-Ar	5	30	
	α Cas	3	100	
11/16/2016	HD 205539	3	1200	
	Th-Ar	5	30	
	ι Peg	3	400	
	Th-Ar	5	30	
	ι Psc	3	400	
	Th-Ar	5	30	
	ζ And	3	400	
	Th-Ar	5	30	
	α Cas	3	100	
	Th-Ar	5	30	
	β Cet	3	400	
Continued on next page				

Table 6.1: List of all observations taken.

Date	Star Name or Exposure Type	Num. of Exposures	Exposure Time (s)	Comments
11/17/2016	HD 205539	3	1200	
	Th-Ar	5	30	
	ι Peg	3	400	
	Th-Ar	5	30	
	ι Psc	3	400	
	Th-Ar	5	30	
	ζ And	3	400	
	Th-Ar	5	30	
	α Cas	3	100	
	β Cet	3	400	
11/19/2016	HD 205539	3	1200	
	Th-Ar	5	30	
	ι Peg	3	400	
	Th-Ar	5	30	
	ι Psc	2	400	Clouds during second exposure
	Th-Ar	5	30	
11/20/2016	HD 205539	3	1200	
	Th-Ar	5	30	
	ι Peg	3	400	
	Th-Ar	5	30	
	ι Psc	3	400	
	Th-Ar	5	30	
	ζ And	3	400	
	Th-Ar	5	30	
	α Cas	3	100	
	β Cet	3	400	
Continued on next page				

Table 6.1: List of all observations taken.

Date	Star Name or Exposure Type	Num. of Exposures	Exposure Time (s)	Comments
	Th-Ar	5	30	
	HD 5638	3	1200	
	Th-Ar	5	30	
	γ Tri	3	400	
11/21/2016	HD 205539	3	1200	
	Th-Ar	5	30	
	ι Peg	3	400	
	Th-Ar	5	30	
	ι Psc	3	400	
	Th-Ar	5	30	
	ζ And	3	400	
	Th-Ar	5	30	
	α Cas	3	100	
	Th-Ar	5	30	
	HD 5638	3	1200	
	Th-Ar	5	30	
	ζ Cas	3	400	
11/27/2016	HD 205539	3	1200	
	Th-Ar	5	30	
	ι Peg	3	400	
	Th-Ar	5	30	
	ι Psc	2	400	Clouds during second exposure
	Th-Ar	5	30	
11/28/2016	HD 205539	3	1200	
	Th-Ar	5	30	
	ι Peg	3	400	
Continued on next page				

Table 6.1: List of all observations taken.

Date	Star Name or Exposure Type	Num. of Exposures	Exposure Time (s)	Comments
	Th-Ar	5	30	
	ι Psc	3	400	
	Th-Ar	5	30	
	ζ And	3	400	
	Th-Ar	5	30	
	α Cas	3	100	
	HD 5638	3	1200	
	Th-Ar	5	30	
	50 Cas	3	400	
12/2/2016	Th-Ar	5	30	
	HD 205539	3	1200	
	Th-Ar	5	30	
	ι Peg	3	400	
	Th-Ar	5	30	
	ι Psc	3	400	
	Th-Ar	5	30	
	ζ And	3	400	
	Th-Ar	5	30	
	α Cas	3	100	
	HD 5638	3	1200	
	Th-Ar	5	30	
	κ Ari	3	400	
	Th-Ar	5	30	
	HD 21278	3	800	
	Th-Ar	5	30	
	11 Tau	3	1200	
Continued on next page				

Table 6.1: List of all observations taken.

Date	Star Name or Exposure Type	Num. of Exposures	Exposure Time (s)	Comments
	Th-Ar	5	30	
	40 Aur	3	800	
	Th-Ar	5	30	
	Sirius	3	30	Saturated
		5	10	Too short
		5	20	
12/3/2016	HD 205539	3	1200	
	Th-Ar	5	30	
	ι Peg	3	400	
	Th-Ar	5	30	
	ι Psc	3	400	
	Th-Ar	5	30	
	ζ And	3	400	
	Th-Ar	5	30	
	α Cas	3	100	
	HD 5638	3	1200	Clouds during last two exposures
	Th-Ar	5	30	
	κ Ari	3	800	Clouds during all exposures
12/4/2016	Th-Ar	5	30	
	HD 205539	3	1200	
	Th-Ar	5	30	
	ι Peg	3	400	
	Th-Ar	5	30	
	ι Psc	3	400	
	Th-Ar	5	30	
Continued on next page				

Table 6.1: List of all observations taken.

Date	Star Name or Exposure Type	Num. of Exposures	Exposure Time (s)	Comments
	ζ And	3	300	
	Th-Ar	5	30	
	α Cas	3	60	
	HD 5638	3	1200	Clouds during last exposure
12/6/2016	Th-Ar	5	30	
	HD 205539	3	1200	
	Th-Ar	5	30	
	ι Peg	3	400	
	Th-Ar	5	30	
	ι Psc	3	400	
	Th-Ar	5	30	
	ζ And	3	300	
	α Cas	3	60	
	HD 5638	3	1200	
	Th-Ar	5	30	
	κ Ari	3	600	Humidity too high to continue
12/10/2016	Th-Ar	5	30	
	HD 205539	3	1200	
	Th-Ar	5	30	
	ι Peg	2	400	Clouds prevented last exposure
	Th-Ar	5	30	
	ζ And	3	300	
	Th-Ar	5	30	
	ι Psc	3	400	Some clouds during first and last exposures
	Th-Ar	5	30	
Continued on next page				

Table 6.1: List of all observations taken.

Date	Star Name or Exposure Type	Num. of Exposures	Exposure Time (s)	Comments
	α Cas	3	60	
	HD 5638	3	1200	Some clouds during last exposure
	Th-Ar	5	30	
	κ Ari	3	600	
	Th-Ar	5	30	
	HD 21278	3	600	
	Th-Ar	5	30	
	11 Tau	3	1200	
	Th-Ar	5	30	
	40 Aur	3	1200	
	Th-Ar	5	30	
12/15/2016	Th-Ar	5	30	
	HD 205539	3	1200	
	Th-Ar	5	30	
	ι Peg	2	400	
	Th-Ar	5	30	
	ι Psc	3	400	
	Th-Ar	5	30	
	ζ And	3	400	
	Th-Ar	5	30	
	α Cas	3	60	
	HD 5638	3	1200	
	Th-Ar	5	30	
	κ Ari	3	600	
	Th-Ar	5	30	
Continued on next page				

Table 6.1: List of all observations taken.

Date	Star Name or Exposure Type	Num. of Exposures	Exposure Time (s)	Comments
	HD 21278	3	600	
	Th-Ar	5	30	
	11 Tau	3	1200	
	Th-Ar	5	30	
	Aldebaran	5	20	
	16 Ori	3	800	
	Th-Ar	5	30	
	40 Aur	3	800	
	Th-Ar	5	30	
	Castor	3	60	
12/16/2016	Th-Ar	5	30	
	HD 205539	3	1200	
	Th-Ar	5	30	
	ι Peg	2	400	
	Th-Ar	5	30	
	ι Psc	3	400	
	Th-Ar	5	30	
	ζ And	3	300	
	Th-Ar	5	30	
	α Cas	3	60	
	HD 5638	1	600	Cut out of observations due to faintness
	κ Ari	3	600	
	Th-Ar	5	30	
	HD 21278	3	600	
12/17/2016	Th-Ar	5	30	
Continued on next page				

Table 6.1: List of all observations taken.

Date	Star Name or Exposure Type	Num. of Exposures	Exposure Time (s)	Comments
	HD 205539	3	1200	
	Th-Ar	5	30	
	ι Peg	2	400	
	Th-Ar	5	30	
	ι Psc	3	400	
	Th-Ar	5	30	
	ζ And	3	300	Too humid to continue

Chapter 7

APPENDIX B - MATLAB CODE

7.1 orbitplot.m

```
function [phase, V] = orbitplot(K,omega,Vo,epa,Per,e,data,gen_or_sp)


omega=omega*pi/180;
mu=2*pi/Per;


%%%Single point
if gen_or_sp==2

    info=fitsinfo(data);
    time_c(1)=info.PrimaryData.Keywords{10,2}+2400000.5;

    for i=1:length(time_c)
        nu_c(i)=kepler(time_c(i),epa,mu,e)*pi/180;
        V(i)=Vo+K*e*cos(omega)+K*cos(omega+nu_c(i));
        phase(i)=(time_c(i)-epa)/Per;
        phase(i)=phase(i)-floor(phase(i));
```

```
        end


%%%Full orbit
elseif gen_or_sp==1
    for k=1:100
        time_p(k)=epa+Per/100*k;
    end


    for i = 1:length(time_p)
        nu_p(i)=kepler(time_p(i),epa,mu,e)*pi/180;
        V(i)=Vo+K*e*cos(omega)+K*cos(omega+nu_p(i));
        phase(i)=0.01*(i-1);
    end
end
```

7.2 TODCOR_m.m

```
function [ vel_shift, v ] = todcor_m(w_f,f,w_g1,g1,w_g2,g2,wrange,...
    nshift,dx,aa,silent)


%modified from IDL code produced by J.R. Davenport


c0=physconst('LightSpeed')*100; %get speed of light in cm/s


if (length(wrange) == 2)
    wmin=wrange(1);
    wmax=wrange(2);
else
    wmin=min(w_f);
    wmax=max(w_f);
end
```

```
wdel=w_f(2)-w_f(1);
a=log10(wmin);
b=log10(wdel/wmin+1);

te=size(w_f);

temp=0:1:te(2)-1;

wlog=10.^(temp*b+a);
wlog=wlog(find(wlog < wmax));



% ; the velocity of each log-linear wavelength pixel
velpix = 2 * c0 * (wlog(101)-wlog(100))/(wlog(101)+wlog(100))



fr  = interp1(w_f,f,wlog);
g1r = interp1(w_g1,g1,wlog);
g2r = interp1(w_g2,g2,wlog);



if isnan(nshift)
    nshift=100;
end

nx=nshift;
ny=nx;
% make big 2-D grid to stuff cross-correlation into
R=zeros(nx*2, ny*2);
```

```matlab
if isnan(dx)
    dx=1;
end

% do the individual 1D cross correlations
lag=nx;
c1=crosscorr(g1r,fr,lag);
c2=crosscorr(g2r,fr,lag);

format long
lag12=2*nx*dx;
N=length(g1r);
sig_g1=sqrt(sum(g1r.^2)./N);
sig_g2=sqrt(sum(g2r.^2)./N);
c12=crosscorr(g2r,g1r,lag12);


if isnan(aa)
    aa=1;
end

alpha=sig_g2/sig_g1*aa;

for i=1:2*nx
    for j=1:2*ny
        R(j,i)=(c1(i)+alpha*c2(j))/sqrt(1+2*alpha*c12(2*nx+(j-i)+1)...
            +alpha^2);
    end
end
```

```
%from two dimensional array, need to return max value and index
%  rmax = max(R,Rmaxind) ; Rmaxindex is subscript of max position
[R_temp,Rmaxindy]=max(R);
[Rmax,Rmaxindx]=max(R_temp);
Rmaxindy(Rmaxindx);
Rmaxindx;
Rmaxind=200*(Rmaxindy(Rmaxindx)-1)+Rmaxindx-1;

figure(1)
contourf(real(R),20)
hold on
plot(Rmaxindx,Rmaxindy)
xlabel('Pixel Shift','FontSize', 22)
ylabel('Pixel Shift','FontSize', 22)
set(gca,'FontSize',22)

vx = mod(Rmaxind,2*nx);
vy = floor(Rmaxind/(2*nx));

fprintf('b = %d  rmax=%d  nx=%d  ny=%d  vx=%d  vy=%d \n', Rmaxind, ...
    Rmax, nx, ny, vx, vy)

% if isnan(silent)
% else
    fprintf('TODCOR: %f %f km/s \n',[vx-nx vy-nx]*velpix/1d5)
% end

v = [-9999 -9999];
```

```
vel_shift = [-9999 -9999];


if vx~=nx
    v(1)=vx;
    vel_shift(1)=(vx-nx)*velpix/1d5;
end
if vy~=nx
    v(2)=vy;
    vel_shift(2)=(vy-nx)*velpix/1d5;

end
```

7.3 correlation_zetaAnd_todcor.m

```
clear all
clc

num_elements=1;

K1=25.2;
K2=-500;
omega1=128;
omega2=omega1+180;
Vo=-23.6;
epa= 2457693.48583;
Per=17.77968;
e=0.01677;


V_std=-3.9;


decd1=24;
```

```
decm1=16;
decs1=01.84;
rad1=00;
ram1=47;
ras1=20.325;

decd2=56;
decm2=37;
decs2=39;
rad2=0;
ram2=41;
ras2=27.2;

dec1=degtorad(1*(decd1+(decm1/60)+(decs1/3600)));
ra1=degtorad(15*(rad1+(ram1/60)+(ras1/3600)));
dec2=degtorad(1*(decd2+(decm2/60)+(decs2/3600)));
ra2=degtorad(15*(rad2+(ram2/60)+(ras2/3600)));

tar = {'20161111-025405-zetaAnd-3x400s.fit',...
    '20161112-021059-zetaAnd-3x400s.fit',...
    '20161116-035224-zetaAnd-3x400s.fit',...
    '20161117-012758-zetaAnd-3x400s.fit',...
    '20161118-021504-zetaAnd-3x400s.fit',...
    '20161121-010204-zetaAnd-3x400s.fit',...
    '20161122-005627-zetaAnd-3x400s.fit',...
    '20161129-010403-zetaAnd-3x400s.fit',...
    '20161203-010853-zetaAnd-3x400s.fit',...
    '20161204-010524-zetaAnd-3x400s.fit',...
    '20161205-005952-zetaAnd-3x300s.fit',...
    '20161207-013941-zetaAnd-3x300s.fit',...
    '20161211-004826-zetaAnd-3x300s.fit',...
```

```
    '20161216-004619-zetaAnd-3x300s.fit',...
    '20161217-015147-zetaAnd-3x300s.fit',...
    '20161218-011523-zetaAnd-3x300s.fit'};

stand = {'20161111-032102-alphaCas-3x100s.fit',...
    '20161112-023613-alfCas-3x100s.fit',...
    '20161116-041654-alfCas-3x100s.fit',...
    '20161117-015431-alfCas-3x100s.fit',...
    '20161118-024047-alfCas-3x100s.fit',...
    '20161121-012751-alfCas-3x100s.fit',...
    '20161122-012522-alfCas-3x100s.fit',...
    '20161129-013019-alfCas-3x100s.fit',...
    '20161203-013528-alfCas-3x100s.fit',...
    '20161204-013556-alfCas-3x100s.fit',...
    '20161205-012214-alfCas-3x60s.fit',...
    '20161207-015716-alfCas-3x60s.fit',...
    '20161211-013253-alfCas-3x60s.fit',...
    '20161216-010848-alfCas-3x60s.fit',...
    '20161217-021125-alfCas-3x60s.fit',...
    '20161217-021125-alfCas-3x60s.fit'};

% tar = {'20161111-025405-zetaAnd-3x400s.fit'};
%
% stand = {'20161111-032102-alphaCas-3x100s.fit'};

% star1 = fopen('zetaAnd.txt','w');

for i=1:length(tar)


    filename_tar=char(tar(i));
```

```
        filename_std=char(stand(i));

        [phase, cor_vel1, cor_vel2, mean_err1, mean_err2, V_c, time]=...
        correlation_todcor(filename_tar,filename_std,dec1,ra1,dec2,ra2,...
        V_std,K1,omega1,K2,omega2,Vo,epa,Per,e,num_elements);

        phase_c1(i)=phase(1);
        phase_c2(i)=phase(2);
        vel1(i)=cor_vel1
        vel2(i)=cor_vel2
        err1(i)=mean_err1
        err2(i)=mean_err2
        O_C1(i)=vel1(i)-V_c(1);
        O_C2(i)=vel2(i)-V_c(2);

%       fprintf(star1,'%f %d %d \n',time(1),cor_vel1,mean_err1);
end




%
[phase_t1, V_t1] = orbitplot(K1,omega1,Vo,epa,Per,e,filename_tar,1);
[phase_t2, V_t2] = orbitplot(K2,omega2,Vo,epa,Per,e,filename_tar,1);
%
figure(18)
errorbar(phase_c1,vel1,err1,'O')
hold on
% errorbar(phase_c2,vel2,err2,'gX')
% hold on
plot(phase_t1,V_t1)
```

```matlab
xlabel('Phase','FontSize', 22)
ylabel('Radial Velocity Shift (km/s)','FontSize', 22)
set(gca,'FontSize',22)
xlim([0 1])

% save('zAndphase.txt','phase_c1','-ascii')
% save('zAndvel1.txt','vel1','-ascii')
% save('zAndvel2.txt','vel2','-ascii')
% save('zAnderr1.txt','err1','-ascii')
% save('zAnderr2.txt','err2','-ascii')

% fclose(star1);

bar=zeros(1,100);

figure(19)
errorbar(phase_c1,O_C1,err1,'O')
hold on
plot(phase_t1,bar,'r-')
xlim([0 1])
xlabel('Phase','FontSize', 22)
ylabel('Radial Velocity Shift (km/s)','FontSize', 22)
set(gca,'FontSize',22)

% figure(15)
% errorbar(phase_c2,O_C2,err2,'gX')
% hold on
% plot(phase_t2,bar,'r-')
% xlim([0 1])
```

7.4 correlation_HD205539_todcor.m

```
clear all
clc

num_elements=2;

K1=52.7017;
K2=61.4873;
omega1=44.885;
omega2=omega1+180;
Vo=-42.1629;
epa= 2457675.57355;
Per=12.19492;
e=0.2949;

V_std=5.3;

decd1=28;
decm1=18;
decs1=57;
rad1=21;
ram1=36;
ras1=25;

decd2=5;
decm2=42;
decs2=57;
rad2=23;
ram2=40;
ras2=43;
```

```matlab
dec1=degtorad(1*(decd1+(decm1/60)+(decs1/3600)));
ra1=degtorad(15*(rad1+(ram1/60)+(ras1/3600)));
dec2=degtorad(1*(decd2+(decm2/60)+(decs2/3600)));
ra2=degtorad(15*(rad2+(ram2/60)+(ras2/3600)));

date_tar = [20161019 20161020 20161024 20161031 20161101 20161111 ...
    20161111 20161116 20161116 20161118 20161119 20161120 20161121 ...
    20161127 20161128 20161202 20161203 20161204 20161206 20161210 ...
    20161215 20161216 20161217];
time_tar = {'013623','011925','011426','012819','012126','005117',...
    '234420','002242','231635','000736','230913','225853','225939',...
    '230243','232836','231428','230827','225914','234558','230705',...
    '225254','235941','232114'};

date_std = [20161118 20161020 20161024 20161031 20161101 20161111 ...
    20161112 20161116 20161117 20161118 20161120 20161121 20161122 ...
    20161128 20161129 20161203 20161204 20161205 20161207 20161211 ...
    20161216 20161217 20161218];
time_std = {'014822','030339','025100','030911','025200','022552',...
    '014527','015723','010228','014822','004002','003305','003046',...
    '003305','003533','004427','004025','003544','011423','010805',...
    '002142', '012731','005106'};

% date_tar = [20161019];
% time_tar = {'013623'};
%
% date_std = [20161118];
% time_std = {'014822'};

% star1 = fopen('HD205539_pri.txt','w');
```

```matlab
% star2 = fopen('HD205539_sec.txt','w');


for i=1:length(date_tar)

    filename_tar = [ num2str(date_tar(i)) '-' char(time_tar(i)) ...
    '-HD205539-3x1200s.fit' ];
    filename_tar=char(filename_tar);
    if i == 11 || i==14
        filename_std = [ num2str(date_std(i)) '-' char(time_std(i)) ...
    '-iotaPsc-2x400s.fit' ];
    else
        filename_std = [ num2str(date_std(i)) '-' char(time_std(i)) ...
    '-iotaPsc-3x400s.fit' ];
    end
    filename_std=char(filename_std);


    [phase, cor_vel1, cor_vel2, mean_err1, mean_err2, V_c, time]=...
    correlation_todcor(filename_tar,filename_std,dec1,ra1,dec2,ra2,...
    V_std,K1,omega1,K2,omega2,Vo,epa,Per,e,num_elements);


    phase_c1(i)=phase(1);
    phase_c2(i)=phase(2);
    time1(i)=time(1);
    time2(i)=time(2);
    vel1(i)=cor_vel1;
    vel2(i)=cor_vel2;
    err1(i)=mean_err1;
    err2(i)=mean_err2;
    O_C1(i)=vel1(i)-V_c(1);
    O_C2(i)=vel2(i)-V_c(2);
```

```matlab
%      fprintf(star1,'%f %d %d \n',time(1),cor_vel1,mean_err1);
%      fprintf(star2,'%f %d %d \n',time(1),cor_vel2,mean_err2);


end



%
[phase_t1, V_t1] = orbitplot(K1,omega1,Vo,epa,Per,e,filename_tar,1);
[phase_t2, V_t2] = orbitplot(K2,omega2,Vo,epa,Per,e,filename_tar,1);
%
figure(13)
errorbar(phase_c1,vel1,err1,'O')
hold on
errorbar(phase_c2,vel2,err2,'gX')
hold on
plot(phase_t1,V_t1,phase_t2,V_t2)
xlabel('Phase','FontSize', 22)
ylabel('Radial Velocity Shift (km/s)','FontSize', 22)
set(gca,'FontSize',22)
xlim([0 1])



% fclose(star1);
% fclose(star2);

bar=zeros(1,100);

figure(14)
errorbar(phase_c1,O_C1,err1,'O')
hold on
```

```
errorbar(phase_c2,O_C2,err2,'gX')
hold on
plot(phase_t1,bar,'r-')
xlim([0 1])
xlabel('Phase','FontSize', 22)
ylabel('Radial Velocity Shift (km/s)','FontSize', 22)
set(gca,'FontSize',22)

% figure(15)
% errorbar(phase_c2,O_C2,err2,'gX')
% hold on
% plot(phase_t2,bar,'r-')
% xlim([0 1])
% xlabel('Phase','FontSize', 16)
% ylabel('Radial Velocity Shift (km/s)','FontSize', 16)
% set(gca,'FontSize',16)
```

7.5 correlation_iotaPeg_todcor.m

```
clear all
clc

num_elements=2;

K1=47.6922;
K2=77.0051;
omega1=150.01;
omega2=omega1+180;
Vo=-5.4463;
epa= 2457671.99867;
Per=10.2023089;
```

```
e=0.00847;


V_std=5.3;


decd1=25;
decm1=20;
decs1=42.4;
rad1=22;
ram1=07;
ras1=0.67;


decd2=5;
decm2=42;
decs2=57;
rad2=23;
ram2=40;
ras2=43;


dec1=degtorad(1*(decd1+(decm1/60)+(decs1/3600)));
ra1=degtorad(15*(rad1+(ram1/60)+(ras1/3600)));
dec2=degtorad(1*(decd2+(decm2/60)+(decs2/3600)));
ra2=degtorad(15*(rad2+(ram2/60)+(ras2/3600)));


date_tar = [20161019 20161020 20161024 20161031 20161101 20161111 ...
    20161112 20161116 20161117 20161118 20161120 20161121 20161122 ...
    20161128 20161128 20161203 20161204 20161205 20161207 20161211 ...
    20161215 20161217 20161218];
time_tar = {'024512','023740','022550','023404','022708','015750',...
    '011815','022156','002132','011231','001416','000427','000617',...
    '000827','230410','001921','001253','001120','005028','001142',...
    '235650','010344','002636'};
```

```
date_std = [20161118 20161020 20161024 20161031 20161101 20161111 ...
    20161112 20161116 20161117 20161118 20161120 20161121 20161122 ...
    20161128 20161129 20161203 20161204 20161205 20161207 20161211 ...
    20161216 20161217 20161218];
time_std = {'014822','030339','025100','030911','025200','022552',...
    '014527','015723','010228','014822','004002','003305','003046',...
    '003305','003533','004427','004025','003544','011423','010805',...
    '002142','012731','005106'};

% date_tar = [20161019];
% time_tar = {'013623'};
%
% date_std = [20161118];
% time_std = {'014822'};

% star1 = fopen('iotaPeg_pri.txt','w');
% star2 = fopen('iotaPeg_sec.txt','w');

for i=1:length(date_tar)

    if i == 20
        filename_tar = [ num2str(date_tar(i)) '-' char(time_tar(i)) ...
    '-iotaPeg-1x400s.fit' ];
    else
        filename_tar = [ num2str(date_tar(i)) '-' char(time_tar(i)) ...
    '-iotaPeg-3x400s.fit' ];
    end
    filename_tar=char(filename_tar);
    if i == 11 || i==14
        filename_std = [ num2str(date_std(i)) '-' char(time_std(i)) ...
```

```
    '-iotaPsc-2x400s.fit' ];
    else
        filename_std = [ num2str(date_std(i)) '-' char(time_std(i)) ...
    '-iotaPsc-3x400s.fit' ];
    end
    filename_std=char(filename_std);


    [phase, cor_vel1, cor_vel2, mean_err1, mean_err2, V_c, time]=...
    correlation_todcor(filename_tar,filename_std,dec1,ra1,dec2,ra2,...
    V_std,K1,omega1,K2,omega2,Vo,epa,Per,e,num_elements);


    phase_c1(i)=phase(1);
    phase_c2(i)=phase(2);
    vel1(i)=cor_vel1
    vel2(i)=cor_vel2
    err1(i)=mean_err1
    err2(i)=mean_err2
    O_C1(i)=vel1(i)-V_c(1);
    O_C2(i)=vel2(i)-V_c(2);

%    fprintf(star1,'%f %d %d \n',time(1),cor_vel1,mean_err1);
%    fprintf(star2,'%f %d %d \n',time(1),cor_vel2,mean_err2);
end



%
[phase_t1, V_t1] = orbitplot(K1,omega1,Vo,epa,Per,e,filename_tar,1);
[phase_t2, V_t2] = orbitplot(K2,omega2,Vo,epa,Per,e,filename_tar,1);
%
figure(13)
```

```
errorbar(phase_c1,vel1,err1,'O')
hold on
errorbar(phase_c2,vel2,err2,'gX')
hold on
plot(phase_t1,V_t1,phase_t2,V_t2)
xlabel('Phase','FontSize', 22)
ylabel('Radial Velocity Shift (km/s)','FontSize', 22)
set(gca,'FontSize',22)
xlim([0 1])

% fclose(star1);
% fclose(star2);

bar=zeros(1,100);

figure(14)
errorbar(phase_c1,O_C1,err1,'O')
hold on
errorbar(phase_c2,O_C2,err2,'gX')
hold on
plot(phase_t1,bar,'r-')
xlim([0 1])
xlabel('Phase','FontSize', 22)
ylabel('Radial Velocity Shift (km/s)','FontSize', 22)
set(gca,'FontSize',22)

% figure(15)
%
% hold on
% plot(phase_t2,bar,'r-')
% xlim([0 1])
```

```
% xlabel('Phase','FontSize', 16)
% ylabel('Radial Velocity Shift (km/s)','FontSize', 16)
% set(gca,'FontSize',16)
```

7.6   earthvelocity_simp.m

```
function [ vearth ] = earthvelocity_simp( dec,ra,jul_date )


[position,velocity]=planetEphemeris(jul_date,'SolarSystem','Earth');
vearth=velocity(1)*cos(dec)*cos(ra)+velocity(2)*cos(dec)*sin(ra)+...
    velocity(3)*sin(dec);


end
```

7.7   kepler.m

```
function [ TA ] = kepler( t,epa,mu,ecc )


m=mu*(t-epa);


if (ecc == 0)
    TA=m*180/pi;
else

    e=m+(ecc*sin(m)/(1-ecc*cos(m)));

    const=sqrt((1+ecc)/(1-ecc));

    TA=(2*atan(const*tan(e/2)))*180/pi;

end
```

```
while(TA < 0)
    TA=TA+360;
end


while(TA > 360)
    TA=TA-360;
end
```

7.8   correlation_alfCas.m

```
clear all

decd1=56;
decm1=37;
decs1=39;
rad1=0;
ram1=41;
ras1=27.2;




dec=degtorad(1*(decd1+(decm1/60)+(decs1/3600)));
ra=degtorad(15*(rad1+(ram1/60)+(ras1/3600)));




stand = {'20161112-023613-alfCas-3x100s.fit',...
    '20161116-041654-alfCas-3x100s.fit',...
    '20161117-015431-alfCas-3x100s.fit',...
    '20161118-024047-alfCas-3x100s.fit',...
```

```
    '20161121-012751-alfCas-3x100s.fit',...
    '20161122-012522-alfCas-3x100s.fit',...
    '20161129-013019-alfCas-3x100s.fit',...
    '20161203-013528-alfCas-3x100s.fit',...
    '20161204-013556-alfCas-3x100s.fit',...
    '20161205-012214-alfCas-3x60s.fit',...
    '20161207-015716-alfCas-3x60s.fit',...
    '20161211-013253-alfCas-3x60s.fit',...
    '20161216-010848-alfCas-3x60s.fit',...
    '20161217-021125-alfCas-3x60s.fit',...
    '20161217-021125-alfCas-3x60s.fit'};

tar = {'20161111-032102-alphaCas-3x100s.fit'};


filename_tar=char(tar);
info_1=fitsinfo(filename_tar);
time1=info_1.PrimaryData.Keywords{10,2}+2400000.5;


for i=1:length(stand)

    filename_std=char(stand(i));

    [save_delt_v, mean_1_2, std_dev, time]=...
    correlation_standard(filename_tar,filename_std,dec,ra);
    time_plot(i)=time-time1;
    vel(i)=mean_1_2;
    err(i)=std_dev;

end

time_b(1)=min(time_plot)-5;
```

```
time_b(2)=max(time_plot)+5;
bar(1)=0;
bar(2)=0;

figure(19)
errorbar(time_plot,vel,err,'O')
hold on
plot(time_b,bar,'r-')
xlim([time_b(1) time_b(2)]);
xlabel(['Time after JD ', num2str(time1), ' (days)'], 'FontSize', 22)
ylabel('Radial Velocity Shift (km/s)','FontSize', 22)
set(gca,'FontSize',22)
```

7.9 correlation_iotaPsc_new.m

```
clear all

decd1=5;
decm1=42;
decs1=57;
rad1=23;
ram1=40;
ras1=43;




dec=degtorad(1*(decd1+(decm1/60)+(decs1/3600)));
ra=degtorad(15*(rad1+(ram1/60)+(ras1/3600)));

date_tar = [20161118];
time_tar = {'014822'};
```

```
date_std = [20161020 20161024 20161031 20161101 20161111 20161112 ...
    20161116 20161117 20161118 20161120 20161121 20161122 20161128 ...
    20161129 20161203 20161204 20161205 20161207 20161211 20161216 ...
    20161217 20161218];
time_std = {'030339','025100','030911','025200','022552','014527',...
    '015723','010228','014822','004002','003305','003046','003305',...
    '003533','004427','004025','003544','011423','010805','002142',...
    '012731','005106'};

filename_tar = [ num2str(date_tar) '-' char(time_tar) ...
    '-iotaPsc-3x400s.fit' ];
info_1=fitsinfo(filename_tar);
time1=info_1.PrimaryData.Keywords{10,2}+2400000.5;

for i=1:length(date_std)

    if i == 10 || i==13
        filename_std = [ num2str(date_std(i)) '-' char(time_std(i)) ...
    '-iotaPsc-2x400s.fit' ];
    else
        filename_std = [ num2str(date_std(i)) '-' char(time_std(i)) ...
    '-iotaPsc-3x400s.fit' ];
    end
    filename_std=char(filename_std);

    [save_delt_v, mean_1_2, std_dev, time]=...
    correlation_standard(filename_tar,filename_std,dec,ra);
    time_plot(i)=time-time1;
    vel(i)=mean_1_2;
    err(i)=std_dev;
```

```
end

time_b(1)=min(time_plot)-5;
time_b(2)=max(time_plot)+5;
bar(1)=0;
bar(2)=0;

figure(20)
errorbar(time_plot,vel,err,'O')
hold on
plot(time_b,bar,'r-')
xlim([time_b(1) time_b(2)]);
xlabel(['Time after JD ', num2str(time1), ' (days)'], 'FontSize', 22)
ylabel('Radial Velocity Shift (km/s)','FontSize', 22)
set(gca,'FontSize',22)
```

7.10 correlation_standard.m

```
function [ save_delt_v, mean_1_2, std_dev, time2 ] = ...
    correlation_standard( fit1,fit2,dec,ra )

save_delt_v=zeros(1,17);
info_1=fitsinfo(fit1);
info_2=fitsinfo(fit2);
time1=info_1.PrimaryData.Keywords{10,2}+2400000.5;
time2=info_2.PrimaryData.Keywords{10,2}+2400000.5;
vearth_1=earthvelocity_simp(dec,ra,time1);
vearth_2=earthvelocity_simp(dec,ra,time2);
vrel=vearth_2-vearth_1;
```

```
for i=1:17
    data_1=fitsread(fit1,'Image',2*i);
    info_1=fitsinfo(fit1);

    cdelt1_1=info_1.Image(1,2*i).Keywords{11,2};
    crval1_1=info_1.Image(1,2*i).Keywords{10,2};
    naxis_1=info_1.Image(1,2*i).Keywords{4,2};

    wavelength_1=zeros(1,naxis_1);
    for k=1:naxis_1
    wavelength_1(1,k)=crval1_1+(k-1)*cdelt1_1;
    end

    lamb_1_trim=find((wavelength_1>(crval1_1+5))&...
    (wavelength_1<(max(wavelength_1)-5)));
    data_1_trim=data_1(lamb_1_trim);
    data_1_trim=data_1_trim-mean(data_1_trim);

%    plot(lamb_1_trim,data_1_trim)

    maxlag=100;

    data_2=fitsread(fit2,'Image',2*i);
    info_2=fitsinfo(fit2);

    cdelt1_2=info_2.Image(1,2*i).Keywords{11,2};
    crval1_2=info_2.Image(1,2*i).Keywords{10,2};
    naxis_2=info_2.Image(1,2*i).Keywords{4,2};

    wavelength_2=zeros(1,naxis_2);
```

```matlab
for k=1:naxis_2
wavelength_2(1,k)=crval1_2+(k-1)*cdelt1_2;
end

lamb_2_trim=find(wavelength_2>(crval1_2+5)&...
wavelength_2<(max(wavelength_2)-5));
data_2_trim=data_2(lamb_2_trim);
data_2_trim=data_2_trim-mean(data_2_trim);

r=crosscorr(data_1_trim,data_2_trim,maxlag);

l_r=length(r);
dwavelength_r=zeros(1,l_r);
v=zeros(1,l_r);

for j=1:l_r
    dwavelength_r(j)=(j-101)*cdelt1_2;
    lam_o=(max(wavelength_2)+min(wavelength_2))/2;
    v(j)=3*10^5*dwavelength_r(j)/(lam_o);
end

r_fit=find(r>0.7);

if(length(r_fit)>3)
    v(r_fit);

    [M,I]=max(r);
    v(I);
%       plot(v,r)

    gauss=fit(v(r_fit).',r(r_fit).','gauss1');
```

```matlab
        coeffvals=coeffvalues(gauss);
%
%        figure(i)
%        plot(gauss,v,r)


    %    plot(v(r_fit),r(r_fit))
    %    title(['Figure ' i])
        save_delt_v(1,i)=coeffvals(2)+vrel;


%        Fitresults=peakfit([v;r],-50,180,2,1,0,15,[-80 15 -5 15],1);
%
%        save_delt_v(1,i)=Fitresults(1,2)+vrel;
    end
end
mean_1_2=mean(save_delt_v);
std_dev=std(save_delt_v);
k=1;
while std_dev>3
    fprintf('standard deviation is greater than tolerance \n')
    m=1;
    while m<=length(save_delt_v)
        if save_delt_v(m)<(mean_1_2-1.5*std_dev) || ...
    save_delt_v(m)>(mean_1_2+1.5*std_dev)
            save_delt_v(m)=[];
            fprintf(['order number ' num2str(m+33) ' is out of bounds \n'])
        end
        m=m+1;
    end
    k=k+1;
    if k>20
```

```
        break
    end
end
mean_1_2=mean(save_delt_v);
std_dev=std(save_delt_v);
% % save_delt_v=save_delt_v(find(save_delt_v>0));
% mean_1_2=mean(save_delt_v);
% std_dev=std(save_delt_v);
end
```

7.11 correlation_todcor.m

```
function [ phase, mean_1, mean_2, mean_err1, mean_err2, V_c, time ] ...
    = correlation_todcor( fit1,fit2,dec1,ra1,dec2,ra2,V_std,K1,omega1,...
    K2,omega2,Vo,epa,Per,e,num_elements)


save_delt_v=zeros(2,17);
info_1=fitsinfo(fit1);
info_2=fitsinfo(fit2);

time1=info_1.PrimaryData.Keywords{10,2}+2400000.5;
time2=info_2.PrimaryData.Keywords{10,2}+2400000.5;
vearth_1=earthvelocity_simp(dec1,ra1,time1);
vearth_2=earthvelocity_simp(dec2,ra2,time2);
vrel=vearth_2-vearth_1;

[phase_c1, V_c1] = orbitplot(K1,omega1,Vo,epa,Per,e,fit1,2);
[phase_c2, V_c2] = orbitplot(K2,omega2,Vo,epa,Per,e,fit1,2);
phase(1)=phase_c1;
phase(2)=phase_c2;
```

```matlab
V_c(1)=V_c1;
V_c(2)=V_c2;

time(1)=time1;
time(2)=time2;

for i=[1 2 3 4 5 6 7 8 9 10 11 12 13 14 15 16 17]
    data_1=fitsread(fit1,'Image',2*i);
    cdelt1_1=info_1.Image(1,2*i).Keywords{11,2};
    crval1_1=info_1.Image(1,2*i).Keywords{10,2};
    naxis_1=info_1.Image(1,2*i).Keywords{4,2};

    wavelength_1=zeros(1,naxis_1);
    for k=1:naxis_1
    wavelength_1(1,k)=crval1_1+(k-1)*cdelt1_1;
    end

    data_2=fitsread(fit2,'Image',2*i);
    info_2=fitsinfo(fit2);

    cdelt1_2=info_2.Image(1,2*i).Keywords{11,2};
    crval1_2=info_2.Image(1,2*i).Keywords{10,2};
    naxis_2=info_2.Image(1,2*i).Keywords{4,2};

    wavelength_2=zeros(1,naxis_2);
    for k=1:naxis_2
    wavelength_2(1,k)=crval1_2+(k-1)*cdelt1_2;
    end

    if num_elements == 1
```

```matlab
    lamb_1_trim=find((wavelength_1>(crval1_1+5))&...
(wavelength_1<(max(wavelength_1)-5)));
    data_1_trim=data_1(lamb_1_trim);
    lamb_1_trim=wavelength_1(lamb_1_trim);
    data_1_trim=data_1_trim-mean(data_1_trim);



    maxlag=100;



    lamb_2_trim=find(wavelength_2>(crval1_2+5)&...
wavelength_2<(max(wavelength_2)-5));
    data_2_trim=data_2(lamb_2_trim);
    lamb_2_trim=wavelength_2(lamb_2_trim);
    data_2_trim=data_2_trim-mean(data_2_trim);

    r=crosscorr(data_2_trim,data_1_trim,maxlag);

    l_r=length(r);
    dwavelength_r=zeros(1,l_r);
    v=zeros(1,l_r);

    for j=1:l_r
        dwavelength_r(j)=(j-101)*cdelt1_2;
        lam_o=(max(wavelength_2)+min(wavelength_2))/2;
        v(j)=3*10^5*dwavelength_r(j)/(lam_o);
    end

    r_fit=find(r>0.7);
```

```matlab
        if(length(r_fit)>3)
            v(r_fit);

            [M,I]=max(r);
            v(I);


            gauss=fit(v(r_fit).',r(r_fit).','gauss1');
%            figure(1)
%
%             plot(gauss,v,r)
%             xlabel('Velocity Shift (km/s)','FontSize', 22)
%             ylabel('Correlation Coefficient','FontSize', 22)
%             set(gca,'FontSize',22)



            coeffvals=coeffvalues(gauss);
            vel_shift(1)=coeffvals(2);
            vel_shift(2)=-9999;
            fprintf('SingleLine: %f km/s \n',vel_shift(1))
        end

    else

    wrange=[min(wavelength_1)+5 max(wavelength_1)-5];
    nshift=NaN;
    dx=NaN;
    aa=1;
    silent=NaN;
```

```
    [vel_shift v] = todcor_m(wavelength_1,data_1,wavelength_2,data_2,...
        wavelength_2,data_2,wrange,nshift,dx,aa,silent);


    end
%     figure(i)
%     figure(1)
%     plot(lamb_1_trim, data_1_trim)
%     figure(2)
%     plot(lamb_2_trim, data_2_trim)
%     [vel_shift v] = todcor_m(lamb_1_trim,data_1_trim,...
% lamb_2_trim,data_2_trim,lamb_2_trim,data_2_trim,wrange,...
%     nshift,dx,aa,silent);


%     if i==1
%         v_sx=v(1);
% %          v_sy=v(2);
%         save_delt_v(1,i)=vel_shift(1)-vrel;
%         save_delt_v(2,i)=vel_shift(2)-vrel;
%     else
%         if v(1) > v_sx-10 && v(1) < v_sx+10
%             save_delt_v(1,i)=vel_shift(1)-vrel;
%             save_delt_v(2,i)=vel_shift(2)-vrel;
%         else
%             save_delt_v(2,i)=vel_shift(1)-vrel;
%             save_delt_v(1,i)=vel_shift(2)-vrel;
%         end
%     end

    vel1=vel_shift(1)-vrel+V_std;
    vel2=vel_shift(2)-vrel+V_std;
```

```matlab
    if abs(V_c1-vel1) > 10 && abs(V_c2-vel2) > 10 && num_elements ~= 1
        save_delt_v(2,i)=vel_shift(1)-vrel+V_std;
        save_delt_v(1,i)=vel_shift(2)-vrel+V_std;
        fprintf('RVs swapped \n')
    else
        save_delt_v(1,i)=vel_shift(1)-vrel+V_std;
        save_delt_v(2,i)=vel_shift(2)-vrel+V_std;
    end


    if save_delt_v(1,i)+vrel-V_std == -9999
        save_delt_v(1,i)=-9999;
    end


    if save_delt_v(2,i)+vrel-V_std == -9999
        save_delt_v(2,i)=-9999;
    end

%          Fitresults=peakfit([v;r],-50,180,2,1,0,15,[-80 15 -5 15],1);
%
%          save_delt_v(1,i)=Fitresults(1,2)+vrel;

end

save_vel1=save_delt_v(1,:);
save_vel1=save_vel1(find(save_vel1~=-9999))
save_vel2=save_delt_v(2,:);
save_vel2=save_vel2(find(save_vel2~=-9999))

% figure(2)
% hist(save_vel1)
```

```matlab
mean_1=mean(save_vel1);
mean_2=mean(save_vel2);
std_dev1=std(save_vel1);
std_dev2=std(save_vel2);
mean_err1=std_dev1/sqrt(length(save_vel1));
mean_err2=std_dev2/sqrt(length(save_vel2));



if num_elements == 1
    k=1;
    while std_dev1>5
        fprintf('standard deviation is greater than tolerance \n')
        m=1;
        while m<=length(save_vel1)
            if save_vel1(m)<(mean_1-2*std_dev1) || ...
                    save_vel1(m)>(mean_1+2*std_dev1)
                save_vel1(m)=[];
%       fprintf(['order number ' num2str(m+33) ' is out of bounds \n'])
                mean_1=mean(save_vel1);
                std_dev1=std(save_vel1);
                mean_err1=std_dev1/sqrt(length(save_vel1));
            else
                m=m+1;
            end
        end
        k=k+1;
        if k>20
            break
        end
    end
```

```
%      mean_2=mean(save_vel2);
%
%      std_dev2=std(save_vel2);
%
%      mean_err2=std_dev2/sqrt(length(save_vel2));


end
end
```

Bibliography

Alan H. Batten. *Binary and multiple systems of stars.* Pergamon Press, 1973.

Leendert Binnendijk. *Properties of double stars: a survey of parallaxes and orbits.* Pennsylvania U.P.; Oxford U.P, 1960.

F. Cochard and O. Thizy. eShel Installation & Maintenance Manual, August 2011. URL `http://www.shelyak-instruments.com/Web/eshel/DC0010C%20eShel%20Installation%20&%20Maintenance%20Manual.pdf`.

James Davenport. todcor.pro, March 2017. URL `https://github.com/jradavenport/jradavenport_idl/blob/master/todcor.pro`.

J. R. Ducati. VizieR Online Data Catalog: Catalogue of Stellar Photometry in Johnson's 11-color system. *VizieR Online Data Catalog*, 2237, 2002.

Thomas Eversberg. Off-the-shelf echelle spectroscopy: Two devices on the test block. *Publications of the Astronomical Society of the Pacific*, 128(969):115001, 2016. URL `http://stacks.iop.org/1538-3873/128/i=969/a=115001`.

F. C. Fekel and J. Tomkin. The double-lined spectroscopic binary IOTA Pegasi. PASP, 95:1000–1005, December 1983. doi: 10.1086/131281.

F. C. Fekel, A. F. Boden, J. Tomkin, and G. Torres. HR 8257: A Three-Dimensional Orbit and Basic Properties. ApJ, 695:1527–1536, April 2009. doi: 10.1088/0004-637X/695/2/1527.

David F. Gray. *The observation and analysis of stellar photospheres. 2. ed.* Cambridge Univ P XVII, 1992.

W. E. Harper. Four double-lined F-type spectroscopic binaries. *Publications of the Dominion Astrophysical Observatory Victoria*, 3:225–245, 1925.

G. Hill. The Measurement of Radial Velocities Using Cross-Correlation Techniques as Applied to Binary Stars. In K.-C. Leung and I.-S. Nha, editors, *New Frontiers in Binary Star Research*, volume 38 of *Astronomical Society of the Pacific Conference Series*, page 127, January 1993.

D. O. Johnson. Spectroscopic Binary Solver. *Journal of Astronomical Data*, 10, December 2004.

Z. Kővári, J. Bartus, K. G. Strassmeier, K. Oláh, M. Weber, J. B. Rice, and A. Washuettl. Doppler imaging of stellar surface structure. XXIII. The ellipsoidal K giant binary ζ Andromedae. A&A, 463:1071–1080, March 2007. doi: 10.1051/0004-6361:20065982.

A. Massarotti, D. W. Latham, R. P. Stefanik, and J. Fogel. Rotational and Radial Velocities for a Sample of 761 HIPPARCOS Giants and the Role of Binarity. AJ, 135:209–231, January 2008. doi: 10.1088/0004-6256/135/1/209.

D. Pourbaix, A. A. Tokovinin, A. H. Batten, F. C. Fekel, W. I. Hartkopf, H. Levato, N. I. Morell, G. Torres, and S. Udry. VizieR Online Data Catalog: SB9: 9th Catalogue of Spectroscopic Binary Orbits (Pourbaix+ 2004-2014). *VizieR Online Data Catalog*, 1, August 2009.

T. Pribulla, Z. Garai, L. Hambálek, V. Kollár, R. Komžík, E. Kundra, J. Nedoroščík, M. Sekeráš, and M Vaňko. Affordable échelle spectroscopy with a 60 cm telescope. *Astronomische Nachrichten*, 336:682, September 2015. doi: 10.1002/asna.201512202.

Daniel J. Schroeder and R. L. Hilliard. Echelle efficiencies: theory and experiment. *Appl. Opt.*, 19(16):2833–2841, Aug 1980. doi: 10.1364/AO.19.002833. URL `http://ao.osa.org/abstract.cfm?URI=ao-19-16-2833`.

S. Zucker and T. Mazeh. Study of spectroscopic binaries with TODCOR. 1: A new two-dimensional correlation algorithm to derive the radial velocities of the two components. ApJ, 420:806–810, January 1994. doi: 10.1086/173605.